Local and regional interactions between tidal stream turbines and coastal environment

Xiaorong Li[a,b,d,*], Ming Li[a], Judith Wolf[c], Alison J. Williams[b], Charles Badoe[b], Ian Masters[b]

[a] *School of Engineering, University of Liverpool, Liverpool, L69 3GQ, UK*
[b] *Faculty of Science and Engineering, Swansea University, Swansea, SA2 8PP, UK*
[c] *National Oceanography Centre, Joseph Proudman Building, 6 Brownlow Street, Liverpool, L3 5DA, UK*
[d] *School of Ocean Sciences, Bangor University, Bangor, LL57 2DG, UK*

Abstract

An extended three-dimensional unstructured ocean model for simulating impacts of tidal stream turbines on tidal current, turbulence and surface waves has been applied to study the interactions between a tidal turbine farm and its surrounding environment. The present study aims to reveal three-dimensional local and regional changes due to the operation of a proposed turbine farm in natural coastal environment. Fine mesh size is assigned at the turbine farm location to capture the details of local wake dynamics, hydrodynamics and suspended sediment transport. Large geographic coverage of the model provides details of changes in regional features. Results showed that the proposed turbine farm comprised of 18 turbines (15-20 m in diameter) with approximately 20% power extraction from the average available power (averaged over five and half tidal cycles) led to local variation of surface elevation within the range of -10 to 3 mm, flow acceleration on both

[*] Corresponding author
Email address: `x.li@bangor.ac.uk` (Xiaorong Li)

sides of the turbine farm, flow acceleration of ~ 0.4 m/s near the bed in the vicinity of the turbine farm which caused bed shear stress to rise up to 2.5 N/m^2 (corresponding to the critical stress of a range of fine gravel and finer sediment particles), locally increased TKE of 0.09 m^2/s^2, reduced wave height of 0.01-0.05 m, and upward sediment transport in the water column. On a regional scale, most of the changes on amplitude and phase of M_2 constituent were observed within 10 km (~ 15 times the array width) from the centre of the turbine farm, and the wake in terms of 95% flow rate recovery was found to be 9 km long (~ 14 times the array width). Noticeable changes were also found in surface waves, bed shear stress and suspended sediment transport on regional scale as result of moderation in tidal and flow dynamics, although much less prominent than the local effects. It is recommended that consideration during the Environmental Impact Assessment stage of tidal stream energy projects should be given to an area that extends beyond the immediate vicinity of the planned turbine farm.

Keywords: Tidal stream energy, Three-dimensional modelling, Environmental Impact Assessment, Local, Regional

1. Introduction

Tidal stream energy, as a resource of clean renewable energy, has been gaining significant attention due to its predictability and widespread availability. According to [1], a total of 20.6 TWh per year could be extracted from 30 key tidal stream sites in the UK. Since the commencement of the MeyGen project in 2010, the total operational tidal stream energy capacity in the UK was 10 MW with 2 MW under construction at the end of 2020. A further 1,000 MW across several sites are also leased for future development [2]. Other countries with significant tidal power potential include Australia, Canada, China, France, South Korea and New Zealand.

To better understand their impacts on the surrounding environment, investigations have been conducted through laboratory experiments and Computational Fluid Dynamics (CFD) simulations around individual turbine structure on local scale ($< 20D$). The major impacts on near-field fluid flow and sediment transport dynamics have been found in three aspects: firstly, flow retardation —water at the immediate downstream region of a turbine normally moves at a lower speed than the free stream due to both energy lose and blockage effect of the device (e.g. [3, 4]); secondly, enhanced mixing —to conserve momentum, the retarded flow expands, causing a cone-shaped expanding region downstream of the turbine known as the wake. Turbulent mixing level is enhanced in the boundary region between the wake and the free stream due to the flow speed gradient and eddy breaking and dissipation [5, 6]. Vortices shed from the tip of the rotor (tip vortices) further enhances the turbulent level in the wake region [7]; and thirdly intensified sediment pick-up —flow features within the near-wake field due to turbine operation can have influence on local bed scour, together with the lee-wake behind the supporting structures. Further detailed studies have also reported on flow acceleration around the energy extraction site [8], velocities below rotor tip and boundary layer in the near wake region [9] and local scouring process [10], among many others.

These detailed experimental and numerical studies mostly focused on local changes around individual turbines. When turbine arrays are employed for more effective power generation, the presence of the farm is expected to raise the overall influence to the ambient fluid flow, turbulence and sediment transport, resulting in much larger scale regional impacts, as revealed by enormous sediment plume tails around offshore wind farms [11]. To assess these potential regional scale processes, coastal and ocean models have been used to simulate the far-field effects of tidal turbine arrays to cover large geographic areas as shown in Table 1. However, due to model resolution and basic assumptions, the near-field process around individual turbine has to be included in these ocean models through certain parameterisations. The simple enhanced flow resistance concept cannot provide correct predictions, especially in the sediment transport modelling point of view [12]. As shown in Table 1, the existing research mostly focused on the potential power generation and flow reduction in horizontal planes. The models used in these research are either two-dimensional or three-dimensional, and the power extraction of tidal turbines is often simulated through adding a depth-averaged retarding force term to the momentum equations of these models. There is a clear lack of understanding of impact of tidal turbine farm on vertical variations of flow dynamics, at both local and regional scale. More importantly, very few studies that investigated changes caused by turbines to sediment transport dynamics took into account the enhanced turbulence mixing within the turbine near field wake, whereas it was found in [13] that without additional modifications to the turbulent closure the predicted turbulence level and bed shear stress are likely to be underestimated.

Through extending the momentum equations and turbulence closure, the individual turbine effects on fluid flow and and sediment suspension have been successfully modelled within the newly developed coastal model of [13, 14]. The present study aims to implement the extended model for large scale tide and wave processes near Irish Sea coast with the presence of turbine array, to reveal the combined local and regional effects on fluid flows, turbulence and sediment transport. The following contents include: a brief description of the the model and setup in section 2; model validation without the turbine array in section 3; results in section 4; discussion of the results in section 5; and conclusions are presented in section 6.

Table 1: Overview of previous studies that assessed far-field impacts of tidal turbine arrays

Author/year	Max. available power	Elevation	Tidal current	Suspended sediment	Bed level
Defne et al. (2011) [15] 3D ROMS Cell size: 180-330 m	5.8 and 11.8 MW for the 20% and 45% removal cases.	1) 45% energy extraction caused changes in maximum water level to spread over the entire domain. Changes in minimum water level were contained in the river channel; 2) Both high and low tide times were delayed. Maximum delay was less than 5 min in the 20% removal case and up to 10 min in the 45% removal case.	1) 20% power removal caused reduction of 0.07 m/s and 0.45 m/s during flood and ebb tide, with an increase of 0.2 m/s in the northern half of the river channel; 2) 40% power removal caused maximum drop of 0.15 m/s and 0.72 m/s during flood and ebb tide. Flow rate increase is limited to 0.25 m/s both over the wetlands and in the northern half of the river channel.		
Ahmadian et al. (2012) [16] 2D DIVAST Cell size: 100 by 100 m	245.5 MW	Changes in water levels were less than 10 cm in the vicinity of the array.	Velocities reduced inside the array, and both upstream and downstream of the array.	1) Concentrations were lower inside the array; 2) Concentrations were changed 15 km away from the array.	
Fallon et al. (2014) [17] 2D DIVAST Cell size: 189 by 189 m	2.88 GW	1) the effects were lower high water level and higher low water level leading to a smaller tidal range. Changes were most severe for the highest density array; high tide was lowered by 23% and low tide was heightened by 30%; 2) the nature of the impacts was the same inside and outside of the array.	Effects were attenuation in the array and acceleration around the array. Changes were greatest for the highest density array; In the farm, reductions in peak ebb and flood velocities were 62% and 32%, while outside the farm, inceases of 39% (ebb) and 33% (flood) were recoreded.		
Thiebot et al. (2015) [18] TELEMAC-2D Cell size: 150 m - 10 km	580 MW	Changes in elevation were smaller than 3 cm.	The mean reduction in flow speed was 0.3 m/s, corresponding to a 15% reduction of the baseline velocity.		
Fairley et al. (2015) [19] 3D MIKE3 FM Cell size:	480 MW				Changes over a tidal cycle was less than 0.2 m.
Robins et al. (2014) [20] TELEMAC 2D Cell size: 15-2000 m	100 MW			The regional impact of energy extraction on bed shear stress was found to be around 0.014 N m^{-2}.	

2. Methodology

2.1. Modelling system

This research is based on a three-dimensional wave-current-sediment fully coupled oceanographic model — the Unstructured Grid Finite Volume Community Ocean Model (FVCOM) [21], and extensions by the authors to represent the interactions between tidal turbine operation and their surrounding environments [13, 14]. For the reason of simplicity, the governing equations of FVCOM are not included here.

In the extended model, the turbine rotation and energy extraction are represented by an additional body force term added to the momentum equations at the computational cells where individual turbines are allocated [13]:

$$F_u = -C_{ext} \cdot \frac{1}{2} \cdot \rho_0 \cdot u \left|\overrightarrow{V}\right| \quad (1)$$

$$F_v = -C_{ext} \cdot \frac{1}{2} \cdot \rho_0 \cdot v \left|\overrightarrow{V}\right| \quad (2)$$

where F_u and F_v are the additional body force terms; C_{ext} is a depth-dependent coefficient that resolves the varying turbine configuration and operation across the water column; ρ_0 is water density; u and v are local velocity components in the x and y directions respectively; $\overrightarrow{V}$ is the local velocity vector and $\left|\overrightarrow{V}\right|$ is the magnitude of the local velocity.

Three turbulence perturbation terms are added to the three-dimensional MY-2.5 turbulence closure to simulate turbine-induced turbulence generation, dissipation and interference for turbulence length-scale [13, 22]:

$$P_{tp} = C_{tp} \cdot \frac{u^3}{\Delta x} \quad (3)$$

$$P_{td} = C_{td} \cdot \frac{u \cdot k}{\Delta x} \tag{4}$$

$$P_l = C_l \cdot P_s \tag{5}$$

where P_{tp} is turbine-induced turbulence generation; P_{td} is turbine-induced turbulence dissipation; P_l is turbine-induced interference for turbulence length-scale; k is turbulent kinetic energy; C_{tp}, C_{td} and C_l are coefficients; P_s is shear production terms of turbulent kinetic energy. Note that horizontal diffusion is calculated using the Smagorinsky's parameterization method.

The wave energy attenuation effects from the array is represented as porous media within SWAN at turbine locations [14]. The porous media absorbs wave energy along a finite line and dissipates it according to a transmission coefficient K_t, hence reduces wave height.

Note that because the values of the coefficients mentioned above are decided empirically through parameter studies, blockage effects are included in the coefficient C_{ext}, instead of being accounted for explicitly in the controlling equations of the model. These coefficients were previously validated against small scale laboratory data [13, 14].

In addition to the above-mentioned modifications, particularly fine grid cells were used around each individual turbine to describe sufficiently the near-field processes, including the change of flow pattern around the structure and associated turbulence characteristics. The model system has been successfully applied to study tidal flow around an individual turbine and the impacts of a single turbine on the local turbulent sediment suspension in the immediate vicinity of the turbine [12]. The present study focuses on the impact of a turbine array to the regional scale hydrodynamics and sediment transport dynamics. For a detailed introduction of the model, one may refer to [21, 13, 14].

2.2. Study site

In this research, the model domain covers a region of the Irish Sea (between 52.808°N and 53.842°N, see Figure 1) to study the potential environmental impact of a tidal turbine array. The Irish Sea is a generally shallow (< 50 m), high-energy shelf sea region, with a central deep trough running north to south [23] (see Figure 2). Within this area, the Anglesey coast in Northwest Wales (red box in Figure 1) features high tidal ranges and large current velocities (> 2.5 m/s during spring tide) as the tidal current here is constricted between the mainland and a group of small rocky islands known as the Skerries [24, 20]. This coastal sea region, therefore, is of high potential to be converted into a tidal stream energy extraction site. In fact, this area has been identified as one of the seven sites of interest for tidal current energy exploitation in the UK [25]. The area around the promontory of Holy Island, known as the West Anglesey Tidal Demonstration Zone (WADZ, Morlais), is planned to host device developers and to provide a maximum of 240MW to the grid [26, 27]. The Holyhead Deep which is approximately 1 km to the west of the WADZ is also of interest to device developers [28]. In this research, the water between the Skerries (see inset of Figure 1) and mainland Anglesey, where the water depth is approximately 20 to 40 m, is selected to implement a turbine farm comprised of 18 turbines (15-20 m in diameter).

Direction of sediment transport around the British Isles was found to be largely determined by the interaction of M_2 and M_4 tides [29]. It was found in ref. [29, 30] that a sediment separation point is located at the south edge

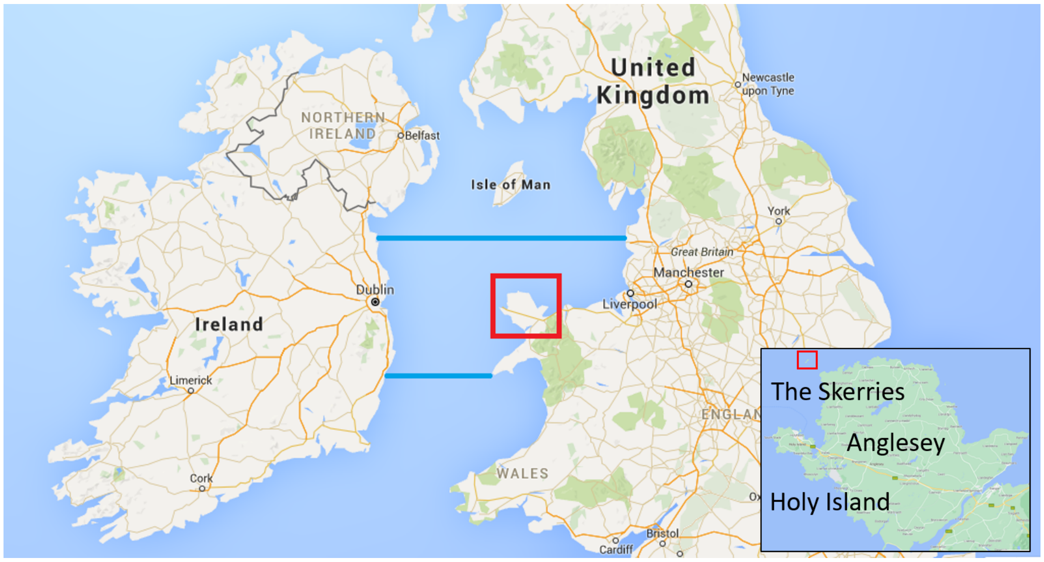

Figure 1: Location of the Anglesey Coast and the study domain of the model. The Anglesey Coast is depicted by the red box and the study domain is enclosed by the blue lines (open boundaries) and two natural coasts. The inset shows the location of the Skerries.

of the study area from where sediments are transported eastward along the Welsh coast to Liverpool Bay and southward to Cardigan Bay, due to tidal asymmetries caused by M_4 constituent. The interaction between M_2 and M_4 tides also leads to strong tidal asymmetry (a strong flood and weaker ebb flow of longer duration) along the Anglesey coast [29], which once perturbed can cause significant changes in sediment transport dynamics (e.g. [31]).

Despite the predominant seabed material off the north coast of Anglesey being recorded as gravel and sand [32], a turbidity maximum with particle size always smaller than 300 μm persisting all year around is observed in this region [33, 34, 35]. Together with the fact that there are no significant river discharges in this area, the source providing fine particles for the Anglesey

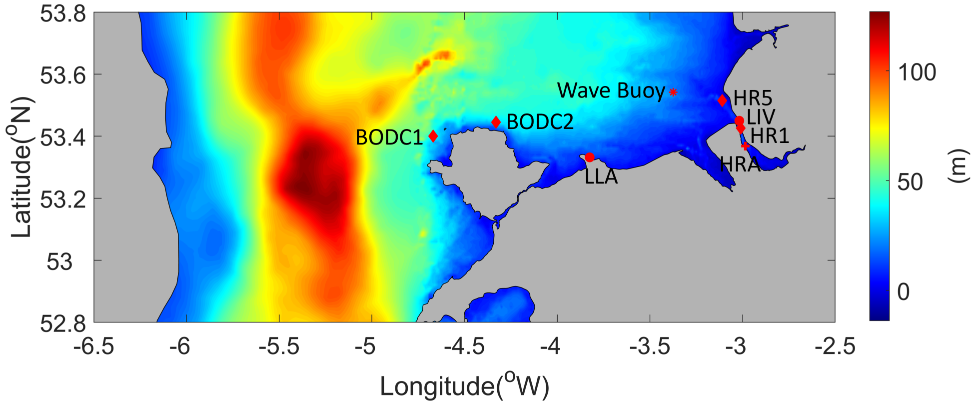

Figure 2: Water depth of the model and locations of validation datasets. Circles are locations of tide gauges; Diamonds are where tidal current data was collected; Star denotes the location of the WaveNet Buoy; Cross indicates where suspended sediment concentration was measured.

Turbidity Maximum (ATM) is unknown. A research investigating the self-maintaining mechanism of the ATM suggested that a closed cycle of large flocs break up into small particles at the core of the maximum where the tidal dissipation is intense and the small particles then re-aggregate into large flocs in the surrounding water where tidal mixing is weaker could be a possible explanation [36]. In which case, disturbance to the local flow and turbulent mixing regimes could potentially break this balance.

As reviewed above, the waters around the Anglesey coast demonstrate interesting flow and sediment transport patterns that may be of importance in relation to water quality, ecological systems and coastal morphology in the local as well as regional areas. Consequently, the Anglesey coast represents an exemplar coastal headland with which to explore the potential environmental impacts of tidal stream energy extraction.

2.3. Model setup

The model domain, enclosed by two natural coasts, East coast of Ireland and the West coast of England, and two open boundaries (blue lines in Figure 1) is discretized into 67,066 triangle elements. The mesh (Figure 3) is refined to a spatial resolution of 100 m around the Anglesey coast and it is further refined to 15-20 m in the Sound between the Skerries and mainland Anglesey to allow turbines to be presented individually. Mesh size increases gradually towards the open boundaries to a resolution of 1600 m. In the vertical direction, the water column is divided into 50 sigma layers with identical layer thickness. Vertical mesh resolution in the region close to the turbine farm, therefore, is approximately 0.4 to 0.8 m. Such high vertical resolution is selected to better resolve the varying turbine configuration. Similar settings have been successfully applied to study the impacts of a single turbine on the local flow field and sediment suspension in the immediate vicinity of the turbine [13, 14, 12].

The bathymetry of the model is extracted from a previous model that covers the West Coast of the United Kingdom [37]. Figure 2 demonstrates the bathymetry of the model with locations of tidal level, tidal current, surface wave and sediment concentration validation data-set imposed.

The model is driven by tidal elevations obtained from harmonic analysis of 15 tidal constituents (M_2 Q_1 O_1 P_1 S_1 K_1 $2N_2$ MU_2 N_2 NU_2 L_2 T_2 S_2 K_2 M_4) extracted from the High Resolution UK Continental Shelf Model (CS20-15HC3) and wave conditions provided by the ECMWF (European Centre for Medium-Range Weather Forecast) 'ERA-Interim' dataset. A time varying uniform wind field based on data measured at the Hilbre Island

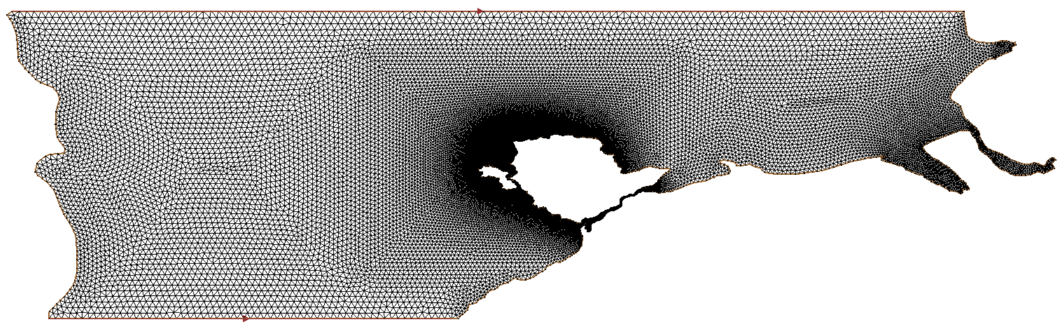

(a) Mesh of the entire domain.

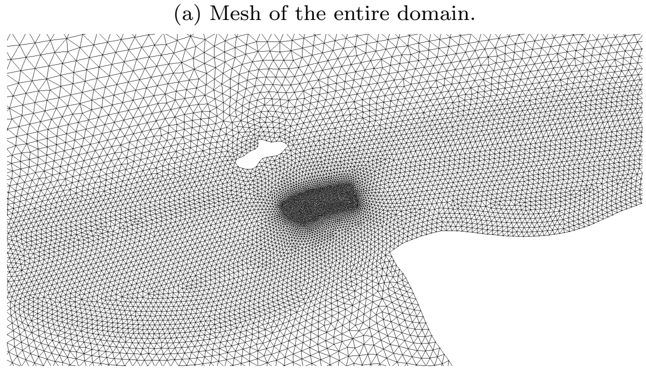

(b) Mesh of the Skerries area.

Figure 3: Mesh of the model. The spatial resolution is 15-20 m in the Sound between the Skerries and mainland Anglesey and 100 m around the Anglesey coast. It increases gradually towards the open boundaries to a resolution of 1600 m.

weather station is used to drive the wave climate. The sediment particle size is specified as D_{50} of 0.22 mm across the entire study domain.

The model is run twice to include a baseline case, i.e. without turbines, and a case incorporating the above-mentioned turbine farm. For the baseline case, the model is run over a month, covering the period from 28/04/2006 00:00:00am to 01/06/2006 00:00:00am. For the case with turbines, the model is run from 17/05/2006 07:00:00am to 20/05/2006 05:00:00am which includes five and a half tidal cycles between Spring and Neap tides. During this time period, wave height peaks at 3.62 m at the selected turbine farm location (Figure 4), representing moderate wave to stormy wave conditions.

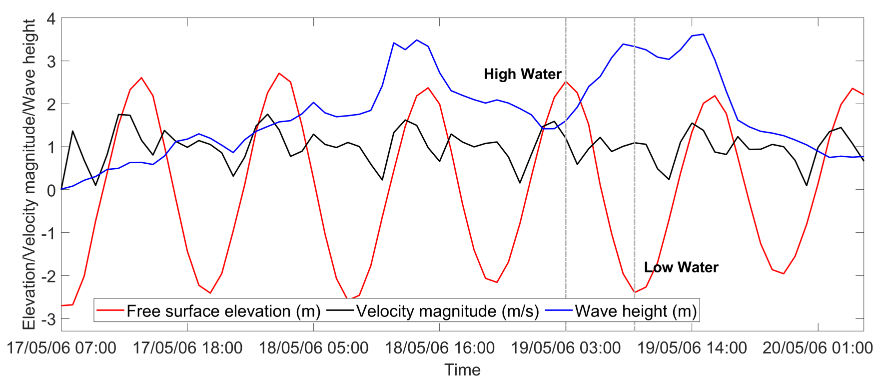

Figure 4: Model calculated free surface elevation, depth-averaged velocity and wave height at the turbine farm location from 17/05/2006 07:00:00am to 20/05/2006 05:00:00am.

Figure 5 shows the tidal ellipses between north-west Anglesey and the Skerries based on depth-averaged velocity, with depth-averaged flow rate at a flood maximum imposed and locations of the tidal turbines highlighted. Location of the device farm is selected based on three factors, i.e. acceptable water depth, large flow rate and high current rectilinearity. The turbine farm is located in the middle of the waterway to minimise its impacts on local shores. The farm consists of 18 turbines, with each represented by an individual mesh cell of 15-20 m in size. Vertically, the turbines are located at the mid-depth. The under keel clearance is 4 m (the difference between the blade tip of the shallowest rotor to lowest astronomical tide). The turbines in the farm are aligned in a staggered manner. They are separated from each other by 8D laterally and 15D in the up/downstream flow direction. Power extraction is estimated to be $\sim 20\%$ of the average available power (averaged over five and half tidal cycles, see Figure 4).

3. Model validation

To validate the model, the model predicted tidal elevation, tidal current and surface waves are compared with measurements at two gauges (LLA and LIV in Figure 2) provided by the UK Tide Gauge Network, current meter data at four locations (HR1, HR5, BODC1 and BODC2 in Figure 2) downloaded from the British Oceanographic Data Centre (BODC), and data collected by a WaveNet buoy (Wave Buoy in Figure 2), respectively. For the reason of simplicity, one may refer to ref. [38] for an in-depth validation of hydrodynamics.

The predicted sediment concentrations at various phases over two tidal processes, spring tide and neap tide, are compared with measurements from a Mersey barrage feasibility study carried out in year 1990 by HR Wallingford [39]. Suspended sediment concentrations were collected at point HRA in Figure 2. The measurements were taken over a spring tide as well as a neap tide at several heights above the seabed.

Figure 6 and Figure 7 present the model predicted and measured flow velocity and suspended sediment concentration at point HRA across the water depth, over tidal cycles of a spring tide and a neap tide. The model results demonstrate a good agreement over the tidal cycles in terms of predicting flow velocity. There are discrepancies in the computed suspended sediment concentration in the region close to the bed surface, which could be attributed to the uncertainties in the local bathymetry and measurements. The measurements were collected sequentially which may lead to imprecision in the timing of the data. In addition, the model used a uniform grain size which may be different from the local sediment size distribution. Further, cohesive sediment is not considered in the present study. Nevertheless, the overall performance of the model in predicting suspended sediment concentration is considered to be good. Root mean square error percentage ($\%_{RMSE}$) calculated based on Equation 6 for velocity and suspended sediment concentration at each moment is listed in Table 2.

$$\%_{RMSE} = \frac{\sqrt{\frac{1}{n}\sum_{i=1}^{n}(q_i - q_{iest})^2}}{q_{max} - q_{min}} \times 100 \tag{6}$$

where n is the number of records in the validation data; q_i is the validation data; q_{iest} is the calculated result; q_{max} and q_{min} are the maximum and minimum records in the calculated result respectively.

4. Results

Through comparing the results of the cases with and without turbines, this section aims to explore the interactions between the turbine farm and its surrounding environment.

Table 2: $\%_{RMSE}$ for velocity and suspended sediment concentration of the model results against field measurements.

	Spring tide				Neap tide			
Time	10:27	11:30	16:37	18:43	7:01	8:57	14:01	16:13
Velocity	38	12	32	35	23	123	10	74
Sediment concentration	87	18	85	51	113	17	21	17

4.1. Surface elevation

The results in this section show free surface elevation changes in the Anglesey coast area caused by the inclusion of the turbine farm at two moments: High Water (HW) and Low Water (LW) indicated in Figure 4. It can be seen from Figure 8a that at HW, the current flows towards the south-west, and the surface elevation around the farm site reduces by up to $\sim$ 10 mm. The reduction continues to be observed west of the Skerries. Elevation decrease is seen at the centres of two eddies, one slightly south-west of the farm and another one off the west coast of Holy island, that exist prior to the inclusion of turbines. Increase of elevation can be seen downstream and further upstream of the device farm, as well as within the Cymyran strait separating Holy island from Anglesey. At LW, when the tidal current flows towards north-east, surface elevation around the turbine farm is increased by up to 3 mm, with a small area of reduction (up to 2 mm) immediately downstream of the turbine farm, where the flow separates as the north-directed flow along the land boundary enters an open area. Changes in surface elevation for the larger area show a similar pattern to the changes at HW, i.e. reduction and increase is observed west and east of the Skerries respectively. These changes, however, are likely to be caused by phase shift of the tide, instead of absolute changes caused by the turbines (see below).

Figure 9 shows the percentage change in the amplitude and phase coefficients of six tidal constituents as a function of distance from the centre of the turbine farm for locations in the area of Figure 8. It can be seen from Figure 9 that for the two dominant tides, M_2 and K_1, changes in amplitude and phase caused by the inclusion of the turbine farm are within 0.5% (i.e. $<$ 12.5 mm for M_2 and $<$ 1.0 mm for K_1) and 0.1% (i.e. $<$ 0.8 min for M_2 and $<$ 1.5 min for K_1) respectively. Percentage change in both amplitude and phase increases as the frequency of the tidal constituent increases. However, because the mean amplitudes of the tidal constituents with higher frequencies are small, large percentage changes of these constituents are not expected to cause significant impact on surface elevation. Impact of the turbine farm on both amplitude and phase is also found to decrease as the distance from the centre of the turbine farm increases. Most of the large changes are observed within 10 km ($\sim$ 16 times the array width) from the centre of the turbine farm.

Figure 10a shows surface elevation with and without the device farm along slice 1 in Figure 5 which is parallel to the flow at HW and LW. The black dotted lines indicate locations where turbines are present. At HW, when flow direction is from 800 m to 0 m, elevation around locations 2 and 3 where turbine is present undergoes a slight increase ($\sim$ 2 mm) followed by a substantial decrease ($\sim$ 8 mm) then an increase back to the undisturbed level. This agrees with the observations of [40]. Similar disturbance to the elevation is also observed at location 1. However, elevation around location 1 is overall smaller than that of the case without turbines, which is attributable to the surface elevation reduction at the downstream end of the farm. Similar influence of turbines on local surface elevation is also observed at LW, when water flows from 0 m to 800 m.

Figure 10b shows surface elevation with and without the device farm along slice 2 in Figure 5 which is perpendicular to the flow at HW and LW. The black dotted lines indicate locations 3D downstream of the five turbines on the second row of array counting from the right-hand side of Figure 5. Therefore, Figure 10b at HW shows influence of the five turbines on surface elevation in the near wake, i.e. an overall reduction in surface elevation. On the other hand, the comparison at LW demonstrates changes surface elevation undergoes at 12D downstream of the second row of devices counting from the left-hand side of Figure 5. It can be seen from the figure that at 12D downstream, fluctuation in surface elevation is very small ($<$ 3 mm), indicating that influence of the upstream devices on elevation has diminished to a negligible level.

4.2. Flow field

Figures 11 and 12 show changes caused by the turbine farm in flow fields at the surface, the mid-layer and the bottom as well as depth-averaged flow fields at HW and LW. At both moments, wake with decelerated flow is observed at the surface layer. Flow acceleration is observed on both sides of the wake, suggesting that the flow is diverted due to the blockage effect of the farm. The accelerated flow jets are also observed in the depth-averaged flow field. They are however much less visible at the mid-layer and the bottom. In comparison with that at the surface, the mid-layer shows the maximum decrease of water velocity because the turbines are located at mid-depth, hence the maximum energy loss. Water at the bottom in the vicinity of the farm is accelerated at both phases of the tide, indicating that the decelerated flow due to the blockage effect of the turbines also navigates its way through the bottom layers. The affected area in terms of water velocity is consistent throughout the water depth and, unlike surface elevation, it mainly follows the flow direction. The magenta lines in Figures 11d and 12d delineate boundaries beyond which velocity recovery is larger than 95%, hence the limit of the wake. The length of the wake is $\sim$ 9.0 km ($\sim$ 450D, i.e. $\sim$ 14 times the width of the turbine farm) at HW and $\sim$ 6.8 km ($\sim$ 340D, i.e. $\sim$ 11 times the width of the turbine farm) at LW. The shorter wake length at LW is caused by a weaker flow.

Figure 13a shows velocity changes through the water depth along slice 1 at HW and LW. Strong flow deceleration is observed at locations where turbines are present at both HW and LW. Wake expansion along the vertical direction is observed within the first 2D ($\sim$ 40 m) of the wake. In this region, flow acceleration occurs below ($\sim$ 0.4 m/s) the wake. After 2D, the size of the wake stays relatively constant until $\sim$ 10D ($\sim$ 200 m) downstream where the wake is mixed from below with the accelerated flow (see region between locations 1 and 2 in Figure 13a at HW). This mixing, however, is not seen at LW, indicating that the individual wakes at LW require a longer distance to recover, potentially due to reduced water depth, hence larger blockage effect.

Figure 13b demonstrates velocity changes across the water depth along slice 2 at HW and LW. The contour at HW shows the wake at 3D downstream of the five turbines on the second row of array counting from the right-hand side of Figure 5. The five turbines are clearly reflected in the figure with decelerated flow centres. Flow rate between two adjacent turbines is also reduced, instead of increased, under the current lateral spacing, therefore leading to strong flow acceleration at the bottom one-third of the water column. The contour at LW shows changes in velocity at 12D downstream of the second row of devices counting from the left-hand side of Figure 5. It can be seen from the figure that velocity reduction after 12D is reduced to $\sim$ 0.1 m/s ($\sim$ 5% deficit), i.e. the five turbines on the third row are no longer operating in the wake of the upstream turbines. However, flow acceleration greater than 0.1 m/s is observed at the bottom one-third of the water column, implying that the influence of the turbines could reach to 3D upstream or further beyond.

4.3. Turbulence kinetic energy

Figures 14 and 15 show changes in TKE at the surface, the mid-layer and the bottom at HW and LW. It can be seen from the figures that the impact of the turbines on TKE is restricted to the local area of the device farm. The wake of each turbine in terms of TKE change stretches up to a distance of approximately 15D and the farm as a whole does not extend the length any longer. As the TKE introduced by the turbines being advected downstream it spreads laterally, forming a cone-shaped highly turbulent area of a maximum width of $\sim$ 8D. The presence of the turbine farm increases local TKE around the devices from nearly 0 to 0.09 m^2/s^2 at the mid-layer. Compared with the mid-layer, TKE enhancement at the other two layers is less significant, but noticeable.

Figure 16a shows TKE changes across the depth along slice 1 at HW and

LW. The inclusion of turbines, as expected, increases TKE in the downstream areas. It is observed that there are two TKE peaks throughout the depth, one above and one below the hub of the turbines. This is because the vortex shed from the tip of the blades is being represented by three turbulence modification terms added to the model. Similar behaviour is reported in [41]. The peaks however almost always occur at $\sim$ 1D ($\sim$ 20 m) downstream of the turbines. This is because even though the three additional turbulence terms are activated at the turbine locations, the velocities at the turbine locations are substantially smaller than those at a certain distance downstream of the turbines, resulting in a rather lower TKE production. The longitudinal stretch of the wake in terms of TKE is in general longer during HW when compared with that during LW. However, it is likely that the wake of most of the turbines has recovered to a very low turbulent level after a distance of 15D ($\sim$ 300 m).

Figure 16b shows TKE changes across the depth along slice 2 at HW and LW. Again, the five turbines on the second row of devices counting from the right-hand side of Figure 5 are clearly shown in the contour at HW. Gaps where TKE is not significantly affected by the presence of the turbines are observed between adjacent devices. At LW, slight increase of TKE is detected in front of the 5 turbines on the second row of devices. TKE between the neighbouring turbines is also slightly increased, indicating that turbulence caused by the turbines on the third row of devices is not yet completely dissipated after a distance of 12D. However, overall, a lateral and longitudinal spacing of 8D and 15D for the current case is sufficient for preventing turbines operating in highly turbulent flows. Note that there is a slight asymmetry in TKE distribution with respect to turbine locations at both HW and LW. This is because Figure 16b shows TKE distribution at a distance downstream of the turbines where the wakes have expanded asymmetrically due to complex local water depth. Because TKE is sensitive to velocity (TKE $\propto U^2$), even though the asymmetry is not obvious in flow field (Figure 13b), TKE distribution can be noticeably asymmetrical.

4.4. Surface waves

Figure 17 shows changes in significant wave height of surface waves at HW and LW. It is observed that at both moments, wave height reduces by a very small amount (0.01-0.05 m, 0.3%-3%) immediately behind the turbines. However, wave height further downstream of the farm is affected by the turbines in opposite ways at HW and LW. During HW, wave height downstream of the farm is reduced by 0.02-0.09 m ($< 7\%$). On the contrary, during LW, wave height downstream of the turbine farm is increased by 0.02-0.13 m ($< 5\%$). Changes in significant wave height are likely to result from a combination of direct impact from the turbine farm and turbine-induced moderation in flow dynamics. In this respect, it is observed that the more significant changes in wave height are along the flow directions and in the downstream of the turbine farm.

4.5. Bed shear stress

Figure 18 shows changes in bed shear stress at HW and LW. It can be seen from the figure that the impact of the turbine farm on bed shear stress is wider than the farm scale. This is because bottom shear stress depends highly on flow velocity and wave height, both of which experience regional changes due to the implementation of the turbine farm. Bed shear stress in the vicinity of the turbine farm is enhanced by up to 2.5 N/m^2, due to the accelerated flow near the bed in the wake. This result agrees with both observations obtained in the laboratory [10, 42, 43, 44] and predictions of three-dimensional CFD simulations [45]. Bed shear stress outside the turbine farm in the wake region, on the other hand, is reduced by ~ 0.3 N/m^2, which agrees with the pattern of the flow field.

Figure 19a shows bed shear stress with and without the turbine farm along slice 1 at HW and LW. It can be seen from the figure that the undisturbed bed shear stress is higher at LW as a result of shallower water depth. Bed shear stress is enhanced by the inclusion of turbines at both moments, and the increase is likely to last longer than the longitudinal spacing (15D, ~ 300 m) between two adjacent turbines at both HW and LW. Both accelerated velocities and enhanced TKE near the bottom contribute to increased bed shear stress [13]. However, changes in TKE at the bottom, as seen in Figure 16a, persist shorter than 15D while increase in velocities near the bottom, as observed in Figure 13a, is still significant after 400 m (20D). Therefore, bed shear stress enhancement in the far field beyond the longitudinal spacing (15D) is likely to be caused solely by flow acceleration.

Figure 19b shows bed shear stress along slice 2 at HW and LW. Again the turbine-induced bed shear stress enhancement is clearly seen at HW, which reflects the near wake impact of the turbines on the second row of devices counting from the right-hand side of Figure 5. Further, it is observed that shear stress in the area between two neighbouring turbines is also enhanced, agreeing with the pattern shown in Figure 13b. Similarly, bed shear stress enhancement seen at LW corresponds to flow dynamics at the same moment and it is likely to reflect the impact of the second row of devices on the shear stress in the upstream area.

4.6. Suspended sediment transport

Figures 20 and 21 show changes caused by the turbine farm in suspended sediment concentration at the surface, the mid-layer and the bottom at HW and LW. At both moments, sediment concentration near the bottom in the vicinity of the turbine farm is reduced (by ~ 4 g/m^3 at HW and ~ 9 g/m^3 at LW, that is $\sim 28\%$ at HW and $\sim 50\%$ at LW) whereas it is increased in the upper part of the water, especially close to the free surface (by ~ 4 g/m^3 at both moments, that is $\sim 146\%$ at HW and $\sim 324\%$ at LW). This agrees with a previous research [12] which studied suspended sediment transport in the wake of a standalone turbine. It was found in [12] that the impact of turbine on suspended sediment transport depends highly on sediment grain size, and when the grain size is 0.22 mm (used in this research) more sediment is mixed from the lower to the upper part of the water column as a result of increased vertical mixing caused by the turbine than that is entrained from the seabed, leading to the reduction of sediment concentration near the bottom.

The wake of the turbine farm in terms of changes in suspended sediment concentration forms an eddy-like pattern off the west coast of Anglesey at HW. A jet of increased suspended sediment concentration, sandwiched by decreased sediment concentration, is clearly observed along the eddy at the surface. A similar pattern is observed at the mid-layer, with the changes being less significant. Sediment concentration in the wake is again decreased near the bottom, although it is increased at the downstream of the eddy.

This eddy-like pattern is not seen at LW. Changes outside the turbine farm are in general one order of magnitude smaller than the changes within the turbine farm.

4.7. Residual sediment transport

This section looks at the impacts of the turbine farm on regional residual sediment transport pathways. Figure 22a shows the residual sediment transport pathways of the baseline case (no turbine farm) around the Anglesey coast, based on calculations of suspended sediment and velocity fields over one tidal cycle from High Water at 19/05/2006 03:00 to the next High Water as shown in Figure 4. One dominant feature of the residual sediment transport observed from the figure is the strong residual sediment transport directed eastwards off the north coast of Anglesey. Similar residual sediment transport within this region are documented in earlier researches [29, 30]. Also, an anti-clockwise eddy-like residual sediment transport is observed in front of the turbine farm location, which is likely caused by the blockage effect of the headland opposite the Skerries on the current.

Figure 22b shows the changes in residual sediment transport caused by the turbine farm. The impact of the farm is far-reaching. The strong residual sediment transport off the north coast of Anglesey observed in the baseline case is reduced by $\sim$ 2.3 kg/m/s ($\sim$ 3%). The sediment transport is reduced by a larger extent just off the coast, east of the headland opposite the Skerries, and the largest reduction in this area is 17.1 kg/m/s ($\sim$ 11%). Further along the coast towards the east, the residual sediment transport which is weak under natural conditions, on the other hand, is increased by $\sim$ 1.6 kg/m/s ($\sim$ 30%). The residual sediment transport rate west of the turbine farm is also enhanced by 8.8 kg/m/s (10%). This could be attributed to the blockage effect caused by the turbine farm.

5. Discussions

5.1. Impacts of tidal turbines

Recent research have shown that impacts of tidal stream energy extraction on coastal environment, marine life, benthic ecology, etc. are evident (e.g. [46]). It is clear that the technological innovations such as tidal turbines need to provide the required energy supply in a manner that protects our invaluable yet fragile environment and ecosystems to safeguard sustainable development.

As a result of high spatial resolution being used and model concept extension, local effects of the turbine farm were revealed by the model. These include variation of surface elevation within the range of -10 to 3 mm, flow acceleration on both sides of the turbine farm, flow acceleration ($\sim$ 0.4 m/s) near the bed in the vicinity of the turbine farm which led to enhanced bed shear stress (up to 2.5 N/m^2), locally increased TKE (0.09 m^2/s^2), locally reduced wave height (0.01-0.05 m), and upward sediment transport in the water column.

Apart from the above-mentioned strong local effects, the turbine farm was also found to have impact on regional hydrodynamics, surface waves and sediment transport dynamics. Most of the changes on the amplitude ($<$ 12.5 mm) and phase ($<$ 0.8 min) of the most dominant tide, M$_2$, were observed within 10 km ($\sim$ 15 times the array width) from the centre of the turbine farm. With a definition of wake edge as 95% flow rate recovery, our results indicate that there are slight wake effects for a distance of around 9 km ($\sim$ 14 times the array width downstream of the device farm). As a consequence of regional scale changes in tidal and flow dynamics, surface waves, bed shear stress and suspended sediment concentration also experienced regional scale modifications, although these regional scale impacts are much less prominent than the local effects (e.g. bed shear stress reduction of $\sim$ 0.3 N/m^2 outside the turbine farm, in contrast to bed shear stress enhancement of 2.5 N/m^2 in the vicinity of the turbine farm). Regional scale impact on residual sediment transport was also observed, with the nature of the impact varying spatially.

The changes in hydrodynamics and sediment transport can cause alterations in light transmission, oxygen supply, waste removal and food availability which once reaching certain thresholds can affect the health of the benthic communities. Therefore, sensitivity of benthic species to both local and regional changes remain an interesting avenue of research, and proper assessment of these impacts are clearly necesseray for each designated site.

5.2. Suspended sediment transport

The Anglesey Turbidity Maximum (ATM) is reported to self-sustain sediment concentrations of 10-15 g/m^3 in winter and $\sim$ 5 g/m^3 in the summer [34]. Compared with this baseline condition, $\sim$ 4 g/m^3 increase in suspended sediment concentration in the upper part of the water attributable to turbine implementation shown in our results is significant. This result, however, is obtained under single particle size (D_{50} = 0.22 mm) settings, whereas the particle size in the ATM ranges from 0 to 0.3 mm. Our result, therefore, can be further refined with a wider distribution of particle sizes.

Note that the area where net sediment transport is affected (Figure 22) is seemingly larger than the area where suspended sediment transport experiences changes (Figures 20 and 21), especially along the north coast of Anglesey. This is because the two moments, i.e. HW and LW, selected to explore the spatial changes caused by the turbine farm may not represent the most significant changes. For instance, when wave height is high, changes in suspended sediment concentration at the three sampling locations are noticeably larger (see Figure 23). It can be observed from Figure 23b that changes in wave height as a result of the implementation of turbines are not cyclic as those in flow velocity (Figure 23a). This is because external influence on waves can be affected by wave direction itself which changes constantly. Two periods of relatively large changes in wave height are observed in Figure 23b outside the HW and LW investigated. These two periods are marked as I and II in Figure 23b and have a duration of around 20 and 10 hours respectively. Maximum percentage changes for periods I and II at three sampling points, intersect of the two slices in Figure 5, P1 in Figure 22B and BODC2, are -34.9%, -32.0%, -25.9% and 11.8%, 10.8%, 6.7%, respectively. Average percentage changes at the three sampling points across the entire period I are -11.0%, -8.9%, -6.2% and 1.0%, 0.7%, 0.6% for period II. The model contains 5 HW and 5 LW events. An average percentage change in wave height is also calculated at the three sampling points for the HW and LW events, and they are -3.4%, -3.3%, -3.1% at HW and -1.1%, 0.1%, 0.01% at LW. These values are also listed in Table 3. Further, as mentioned in Section 4.1, impact of the turbine farm on tidal conditions can reach as far as 10 km which can contribute to the observed regional scale changes on net sediment transport.

The balance between the strong mixing in the ATM and the weaker mix-

Table 3: Maximum and average percentage changes in wave height at three sampling points for different time periods. The three sampling points are intersect of the two slices in Figure 5 (abbreviated as I in the table), P1 in Figure 22B and BODC2. Time periods include periods I and II in Figure 23b and HW and LW events in Figure 4.

	Period I			Period II			HW			LW		
	I	P1	BODC2	I	P1	BODC2	I	P1	BODC2	I	P1	BODC2
Max	-34.9%	-32.0%	-25.9%	11.8%	10.8%	6.7%	-	-	-	-	-	-
Mean	-11.0%	-8.9%	-6.2%	1.0%	0.7%	0.6%	-3.4%	-3.3%	-3.1%	-1.1%	0.1%	0.01%

ing in the surrounding waters has been proposed to be the mechanism behind the self-sustained ATM [36]. This hypothesis was supported by observations of fluxes of particles in the range 0-0.08 mm to diffuse out of the ATM and fluxes of particles in the range 0.08-0.25 mm to diffuse into the ATM. As an endeavour to explore the capabilities of the model in use to simulate these phenomena and hence the consequences of turbine-induced disturbances to flow field and mixing on the ATM, an additional test case was carried out in which the particle size was set to 0.04 mm to represent the finer sediment group (i.e. particles in the range 0-0.08 mm). Net fluxes calculated at the location indicated in Fig.2 of [34], however, suggested outward sediment transport from the ATM for both sediment groups (0-0.08 and 0.08-0.25 mm). This is likely to be caused by the discrepancies between the processes the model considers and the dominant processes that govern the local recycle of sediment. In particular, the local recycle of sediment is mainly driven by advection and diffusion, whereas the model also takes erosion into consideration.

5.3. Limitation of the model

Uncertainties are expected in the results from the modelling simulations in the present study. First of all, due to data availability, the model is validated against measurements collected at a limited number of locations. In particular, LIV, HR1, HR5 and HRA are at sheltered locations while the tidal stream energy site is more remote and exposed. It is, therefore, a reasonable concern whether the model is producing accurate results at the farm site, even though three of the data collection sites, LLA, BODC1 and BODC2, are close to the turbine farm. This is because current and waves are largely affected by local bathymetry, coastline shape, and so on. Current and waves, on the other hand, drive sediment transport which shows some discrepancies against measurements (see Figures 6 and 7). As mentioned above, apart from hydrodynamics, this could be caused by the fact that a uniform grain size is used in the model while local sediment is a mix of particles with different sizes. However, despite the shortcomings, the model predicted sediment concentration profiles show good agreement with the measurements according to the $\%_{RMSE}$ values in Table 2, especially considering that, instead of averaged over time, the measurements are collected instantly which can cause timing errors.

Further, due to lack of data, the ambient turbulence is not validated against measurements. Indeed, tidal stream energy sites often feature high turbulence and the characterization of which is critical for the design of individual turbines and turbine farms [47]. In particular, higher turbulence intensity leads to faster wake recovery [48]. However, the turbulence closure in use is a widely-used model which can produce accurate turbulent mixing if the flow field (which is validated) and density field (beyond the remit of this paper) are accurate. Further, the turbine induced perturbation on turbulence is very large compared to the background turbulence. For example, the data of [49] indicates that turbulence in the near wake is $\sim 600\%$ larger than the baseline turbulence. Therefore, turbulence transported and dissipated in the wake is mainly turbulence caused by the turbines which is accurately simulated by the three additional turbulence perturbation terms, and errors in the background turbulence plays a small role. Nevertheless, in-situ surveys of ambient turbulence characteristics and validation of modelled ambient turbulence are recommended as an important and interesting avenue of investigation in future research.

Finally, a particular turbine design in one array layout is examined in the present study. The focus is to explore the combined local and regional impacts from a typical tidal array deployment in coastal environment. The qualitative assessments, however, are clearly indicative to the more general practice in other sites with different hydro- and morphodynamic conditions. Further, the model is able to simulate other turbine designs, array layouts and locations. For instance, ref. [50] applied the model to study the environmental impact of different array layouts and turbulence levels in the Pentland Firth. Nevertheless, case studies that focus on the impact of different turbines and array layouts on the wake and subsequently the environment can be explore further in future research.

6. Conclusions

A three-dimensional unstructured ocean model with additional terms for simulating impacts of tidal turbines on current, turbulence and surface waves has been applied to study the interactions between a tidal turbine farm and the surrounding environment. Using a region of the Irish Sea as a case study with a turbine farm implemented in high resolution in the water between the Skerries and mainland Anglesey, the results revealed:

1) local impact of the turbine farm including variation of surface elevation, flow acceleration on both sides of the turbine farm, flow acceleration near the bed in the vicinity of the turbine farm which leads to enhanced bed shear stress, locally increased TKE, locally reduced wave height and upward sediment transport in the water column. It is, however, important to assess the significance of these changes relative to natural variability;

2) the turbine farm can have impact on regional hydrodynamics, surface waves and suspended sediment transport, although these regional scale impacts are much less prominent than the local effects. Therefore, consideration should be given to an area that extends beyond the immediate vicinity of the planned turbine farm. In addition, it can also lead to enhanced sediment deposition along the local shorelines.

3) the model in use can reveal wake dynamics of turbines, including wake expansion along the vertical direction as well as the length and horizontal expanse of wakes, which can support decision-making related to array planning, although the precision requires further validations.

4) simulation of suspended sediment transport with multiple grain size and sensitivity of benthic species to both local and regional changes would

be interesting topics for future research.

Acknowledgement

This work is part of the Selkie project, funded by the European Union's European Regional Development Fund through the Ireland Wales Cooperation programme. X. Li would like to acknowledge support from the Chinese Scholar Council and the University of Liverpool.

References

[1] Department for Business, Energy and Industrial Strategy, Energy innovation needs assessment. sub-theme report: Tidal stream. technical report. (accessed: 30.04.2021).
URL https://assets.publishing.service.gov.uk/government/uploads/system/upload

[2] G. Smart, M. Noonan, Tidal stream and wave energy cost reduction and industrial benefit (2018).

[3] L. Myers, A. Bahaj, An experimental investigation simulating flow effects in first generation marine current energy converter arrays, Renewable Energy 37 (1) (2012) 28–36.

[4] F. Maganga, G. Germain, J. King, G. Pinon, E. Rivoalen, Experimental characterisation of flow effects on marine current turbine behaviour and on its wake properties, IET Renewable Power Generation 4 (6) (2010) 498–509.

[5] L. Myers, A. Bahaj, Experimental analysis of the flow field around horizontal axis tidal turbines by use of scale mesh disk rotor simulators, Ocean Engineering 37 (2) (2010) 218–227.

[6] Y. Chen, J. Sun, B. Lin, J. Lin, J. Guo, Spatial evolution and kinetic energy restoration in the wake zone behind a tidal turbine: An experimental study, Ocean Engineering 228 (2021) 108920.

[7] S. PM Sforza, M. Smorto, Three-dimensional wakes of simulated wind turbines, AIAA Journal 19 (9) (1981) 1101–1107.

[8] X. Sun, J. Chick, I. Bryden, Laboratory-scale simulation of energy extraction from tidal currents, Renewable Energy 33 (6) (2008) 1267–1274.

[9] L. Chen, W.-H. Lam, Slipstream between marine current turbine and seabed, Energy 68 (2014) 801–810.

[10] C. Hill, M. Musa, L. P. Chamorro, C. Ellis, M. Guala, Local scour around a model hydrokinetic turbine in an erodible channel, Journal of Hydraulic Engineering 140 (8) (2014) 04014037.

[11] Q. Vanhellemont, K. Ruddick, Turbid wakes associated with offshore wind turbines observed with landsat 8, Remote Sensing of Environment 145 (2014) 105–115. doi:10.1016/j.rse.2014.01.009.
URL `http://dx.doi.org/10.1016/j.rse.2014.01.009`

[12] X. Li, M. Li, L. O. Amoudry, R. Ramirez-Mendoza, P. D. Thorne, Q. Song, P. Zheng, S. M. Simmons, L.-B. Jordan, S. J. McLelland, Three-dimensional modelling of suspended sediment transport in the far wake of tidal stream turbines, Renewable Energy 151 (2020) 956–965.

[13] X. Li, M. Li, S. J. McLelland, L.-B. Jordan, S. M. Simmons, L. O. Amoudry, R. Ramirez-Mendoza, P. D. Thorne, Modelling tidal stream turbines in a three-dimensional wave-current fully coupled oceanographic model, Renewable Energy (2017).

[14] X. Li, M. Li, L.-B. Jordan, S. McLelland, D. R. Parsons, L. O. Amoudry, Q. Song, L. Comerford, Modelling impacts of tidal stream turbines on surface waves, Renewable energy 130 (2019) 725–734.

[15] Z. Defne, K. A. Haas, H. M. Fritz, Numerical modeling of tidal currents and the effects of power extraction on estuarine hydrodynamics along the georgia coast, usa, Renewable Energy 36 (12) (2011) 3461–3471.

[16] R. Ahmadian, R. Falconer, B. Bockelmann-Evans, Far-field modelling of the hydro-environmental impact of tidal stream turbines, Renewable Energy 38 (1) (2012) 107–116.

[17] D. Fallon, M. Hartnett, A. Olbert, S. Nash, The effects of array configuration on the hydro-environmental impacts of tidal turbines, Renewable Energy 64 (2014) 10–25.

[18] J. Thiébot, P. B. du Bois, S. Guillou, Numerical modeling of the effect of tidal stream turbines on the hydrodynamics and the sediment transport–application to the alderney race (raz blanchard), france, Renewable Energy 75 (2015) 356–365.

[19] I. Fairley, I. Masters, H. Karunarathna, The cumulative impact of tidal stream turbine arrays on sediment transport in the pentland firth, Renewable Energy 80 (2015) 755–769.

[20] P. E. Robins, S. P. Neill, M. J. Lewis, Impact of tidal-stream arrays in relation to the natural variability of sedimentary processes, Renewable Energy 72 (2014) 311–321.

[21] C. Chen, H. Liu, R. C. Beardsley, An unstructured grid, finite-volume, three-dimensional, primitive equations ocean model: application to coastal ocean and estuaries, Journal of atmospheric and oceanic technology 20 (1) (2003) 159–186.

[22] T. Roc, D. C. Conley, D. Greaves, Methodology for tidal turbine representation in ocean circulation model, Renewable Energy 51 (2013) 448–464.

[23] K. J. Horsburgh, A. E. Hill, A three-dimensional model of density-driven circulation in the irish sea, Journal of Physical Oceanography 33 (2) (2003) 343–365.

[24] M. Dobson, W. Evans, K. James, The sediment on the floor of the southern irish sea, Marine Geology 11 (1) (1971) 27–69.

[25] Black Veatch (2005), Tidal stream - phase ii uk tidal stream energy resource assessment, A report to the Carbon Trust's Marine Energy Challenge (2005).

[26] Marine Energy Wales, West anglesey tidal demonstration zone. (accessed: 10.03.2021).
URL `https://www.marineenergywales.co.uk/marine-energy-in-wales/demonstration-`

[27] M. Lewis, S. Neill, P. Robins, M. R. Hashemi, S. Ward, Characteristics

of the velocity profile at tidal-stream energy sites, Renewable Energy 114 (2017) 258–272.

[28] D. Potter, Alteration to the shallow-water tides and tidal asymmetry by tidal-stream turbines, Lancaster University (United Kingdom), 2019.

[29] R. Pingree, D. Griffiths, Sand transport paths around the british isles resulting from m 2 and m 4 tidal interactions, Journal of the Marine Biological Association of the United Kingdom 59 (02) (1979) 497–513.

[30] A. H. Stride, Sediment transport by the north sea, E. Goldberg (Ed.), North Sea Science, M.I.T. Press (1973) 101–130.

[31] S. P. Neill, E. J. Litt, S. J. Couch, A. G. Davies, The impact of tidal stream turbines on large-scale sediment dynamics, Renewable Energy 34 (12) (2009) 2803–2812.

[32] N. Golding, M. A. Vincent, D. W. Connor, The Irish Sea Pilot: Report on the development of a Marine Landscape classification for the Irish Sea, Joint Nature Conservation Committee, 2005.

[33] D. Bowers, S. Gaffney, M. White, P. Bowyer, Turbidity in the southern irish sea, Continental Shelf Research 22 (15) (2002) 2115–2126.

[34] D. Bowers, K. Ellis, S. Jones, Isolated turbidity maxima in shelf seas, Continental Shelf Research 25 (9) (2005) 1071–1080.

[35] E. Van der Lee, D. Bowers, E. Kyte, Remote sensing of temporal and spatial patterns of suspended particle size in the irish sea in relation

to the kolmogorov microscale, Continental Shelf Research 29 (9) (2009) 1213–1225.

[36] K. Ellis, C. Binding, D. Bowers, S. Jones, J. Simpson, A model of turbidity maximum maintenance in the irish sea, Estuarine, Coastal and Shelf Science 76 (4) (2008) 765–774.

[37] R. Burrows, I. Walkington, N. Yates, T. Hedges, J. Wolf, J. Holt, The tidal range energy potential of the west coast of the united kingdom, Applied Ocean Research 31 (4) (2009) 229–238.

[38] X. Li, M. Li, J. Wolf, A. J. Williams, C. Badoe, I. Masters, A three-dimensional regional scale model for tidal stream turbine implementation and impact assessment, in: Submitted to the Proceedings of the European Wave and Tidal Energy Conference, Plymouth, UK, 2021.

[39] HR Wallingford, Mersey barrage feasibility study: stage ii, Hydraulic and sedimentation study, sand flux measurement, Report EX 2225 (1990) 193–196.

[40] L. Myers, A. Bahaj, Wake studies of a 1/30th scale horizontal axis marine current turbine, Ocean engineering 34 (5-6) (2007) 758–762.

[41] S. Tedds, I. Owen, R. Poole, Near-wake characteristics of a model horizontal axis tidal stream turbine, Renewable Energy 63 (2014) 222–235.

[42] L.-B. Jordan, S. M. Simmons, S. J. McLelland, B. J. Murphy, D. R. Parsons, L. Murdoch, The impact of tidal stream turbines on 3D flow and bed shear stress measured with particle image velocimetry in a

laboratory flume, in: Proceedings of the 11th European Wave and Tidal Energy Conference, Nantes, France, 2015, pp. 654–660.

[43] M. Musa, C. Hill, F. Sotiropoulos, M. Guala, Performance and resilience of hydrokinetic turbine arrays under large migrating fluvial bedforms, Nature Energy 3 (10) (2018) 839–846.

[44] M. Musa, C. Hill, M. Guala, Interaction between hydrokinetic turbine wakes and sediment dynamics: array performance and geomorphic effects under different siting strategies and sediment transport conditions, Renewable Energy 138 (2019) 738–753.

[45] S. Sufian, Numerical modeling of impacts from horizontal axis tidal turbines, Ph.D. thesis, School of Engineering, University of Liverpool (6 2016).

[46] S. Fraser, V. Nikora, B. J. Williamson, B. E. Scott, Hydrodynamic impacts of a marine renewable energy installation on the benthic boundary layer in a tidal channel, Energy Procedia 125 (2017) 250–259.

[47] S. P. Neill, K. A. Haas, J. Thiébot, Z. Yang, A review of tidal energyresource, feedbacks, and environmental interactions, Journal of Renewable and Sustainable Energy 13 (6) (2021).

[48] C. E. Badoe, X. Li, A. J. Williams, I. Masters, Output of a tidal farm in yawed flow and varying turbulence using gad-cfd, Ocean Engineering 294 (2024) 116736.

[49] M. Harrison, W. Batten, L. Myers, A. Bahaj, Comparison between cfd simulations and experiments for predicting the far wake of horizontal

axis tidal turbines, IET Renewable Power Generation 4 (6) (2010) 613–627.

[50] S. Zazzini, M. De Dominicis, A. Pini, G. Leuzzi, P. Monti, R. O'Hara Murray, X. Li, Turbulence changes due to a tidal stream turbine operation in the pentland firth (scotland, uk), in: International workshop on Metrology for the Sea, Genoa, Italy, 2019, pp. 309–314.

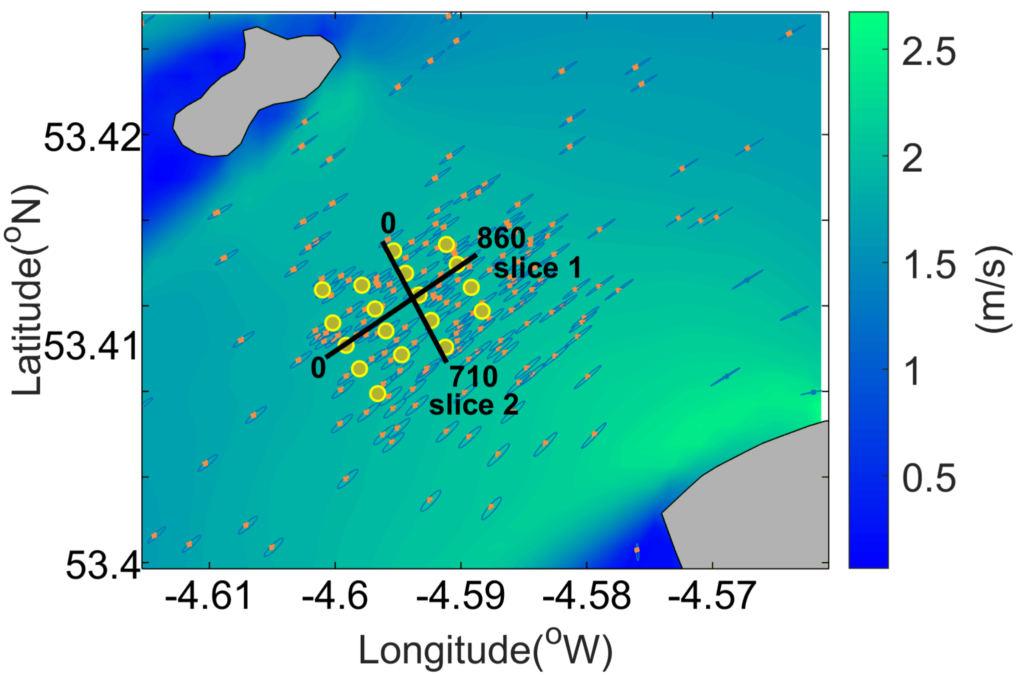

Figure 5: Tidal ellipses between north-west Anglesey and the Skerries imposed on depth-averaged velocity at a flood maximum. Locations of turbines are depicted by filled circles. They are separated from each other by 8D laterally and 15D in the up/downstream flow direction. The two black solid lines indicate locations at which trend lines of free surface elevation and bed shear stress, and vertical contours of velocity and TKE are drawn in Section 4.

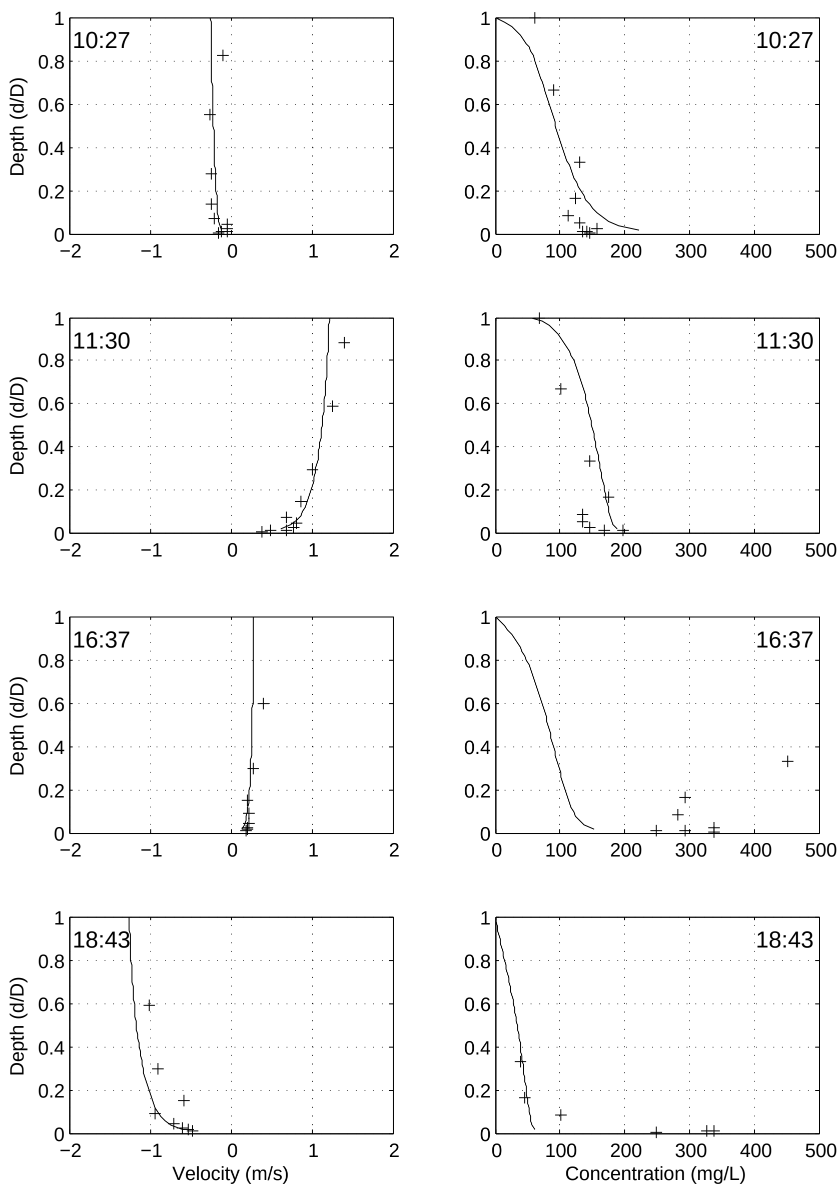

Figure 6: Comparison of model predicted and measured flow velocity and suspended sediment concentration at different height above the bed at point HRA over a spring tide. Four panels on the left-hand side are flow velocity profiles and the other four panels on the right-hand side are suspended sediment concentration profiles. The solid lines denote model calculated values and the symbols are for the measured results.

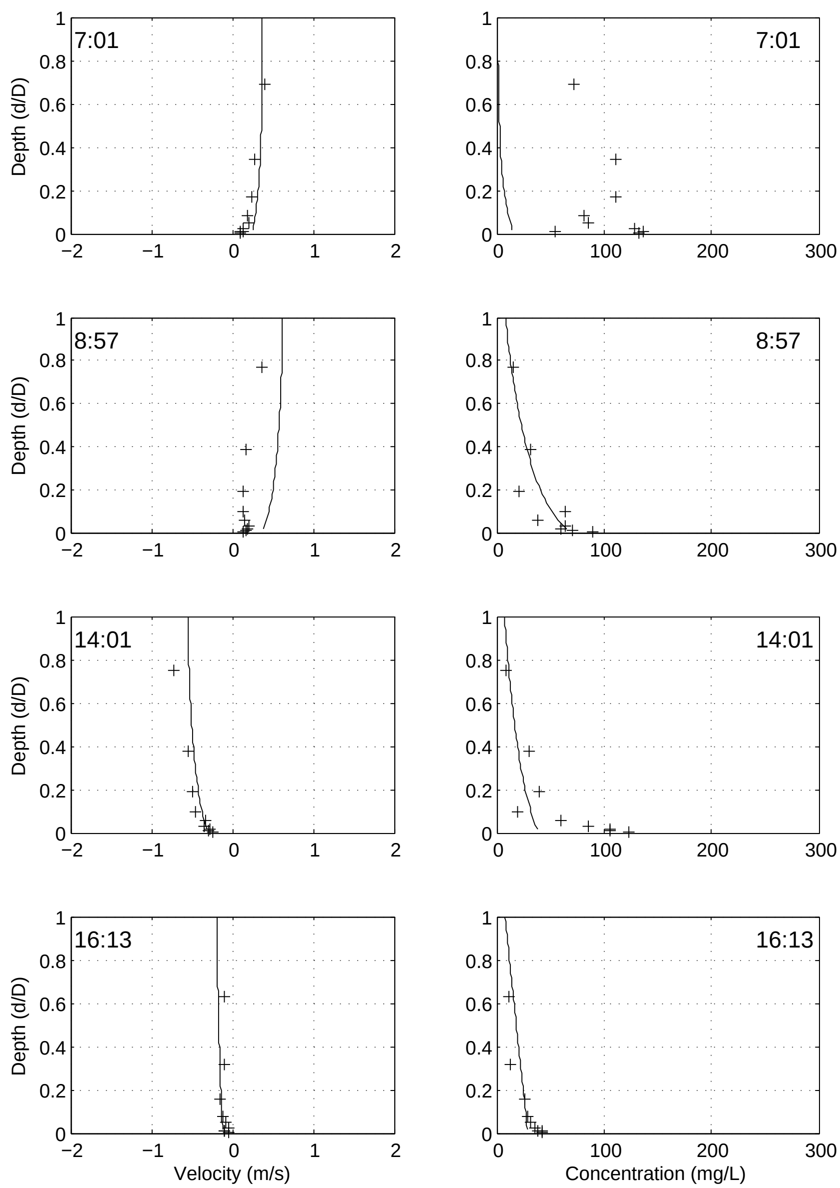

Figure 7: Comparison of model predicted and measured flow velocity and suspended sediment concentration at different height above the bed at point HRA over a neap tide. Four panels on the left-hand side are flow velocity profiles and the other four panels on the right-hand side are suspended sediment concentration profiles. The solid lines denote model calculated values and the symbols are for the measured results.

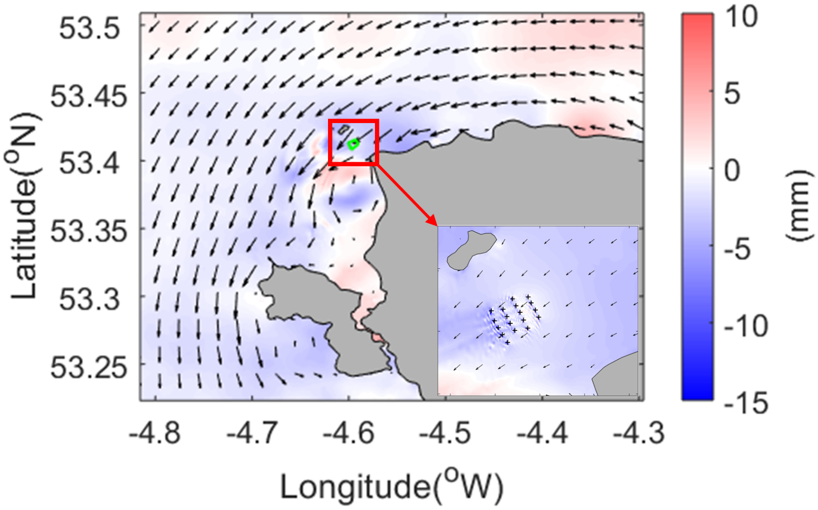

(a) HW

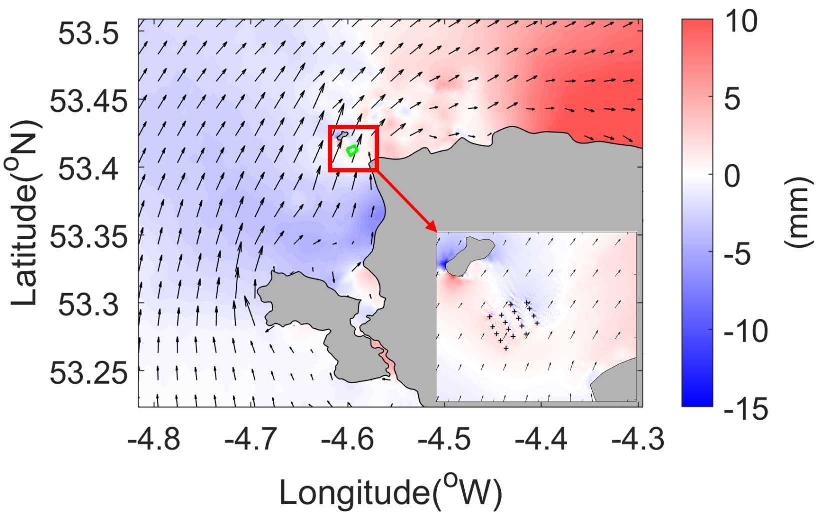

(b) LW

Figure 8: Surface elevation change. Arrows are imposed to indicate flow directions.

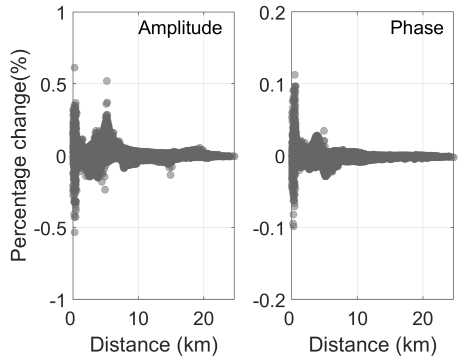

(a) K_1. Mean amplitude is 0.203 m.

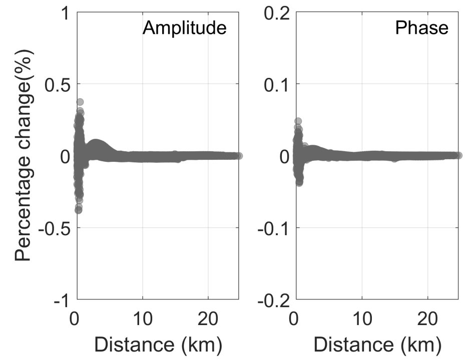

(b) M_2. Mean amplitude is 2.459 m.

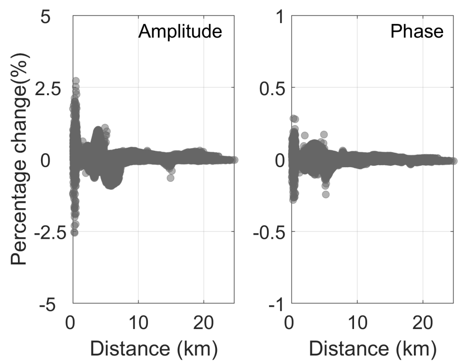

(c) M_3. Mean amplitude is 0.049 m.

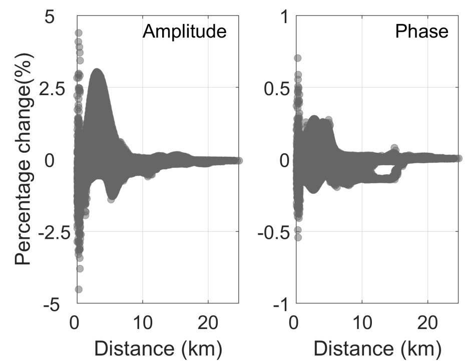

(d) M_4. Mean amplitude is 0.087 m.

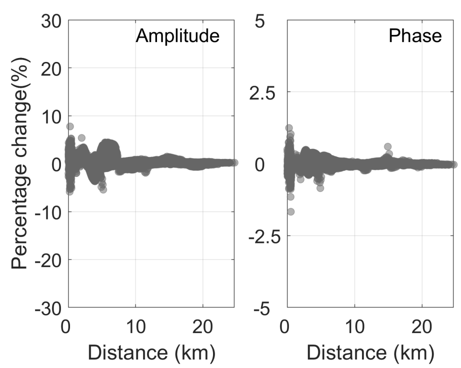

(e) $2MK_5$. Mean amplitude is 0.011 m.

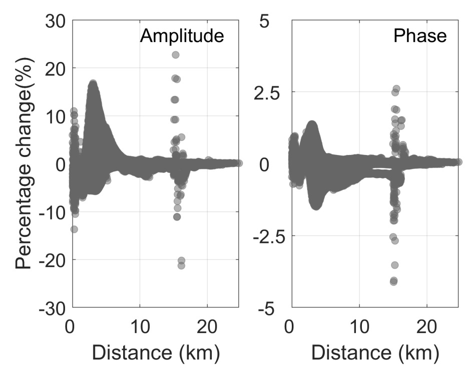

(f) M_6. Mean amplitude is 0.019 m.

Figure 9: Percentage change in the amplitude and phase coefficients of six tidal constituents.

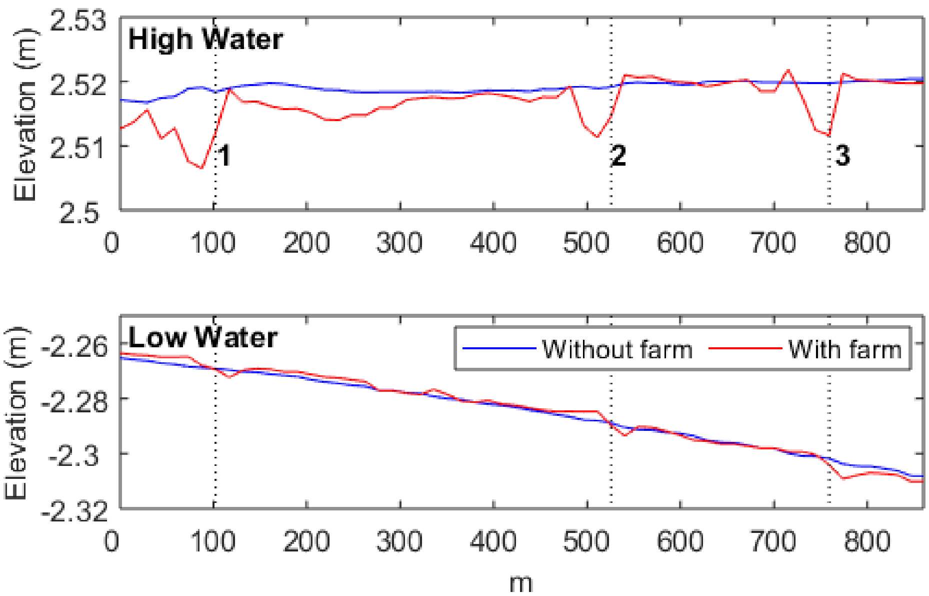

(a) Slice 1

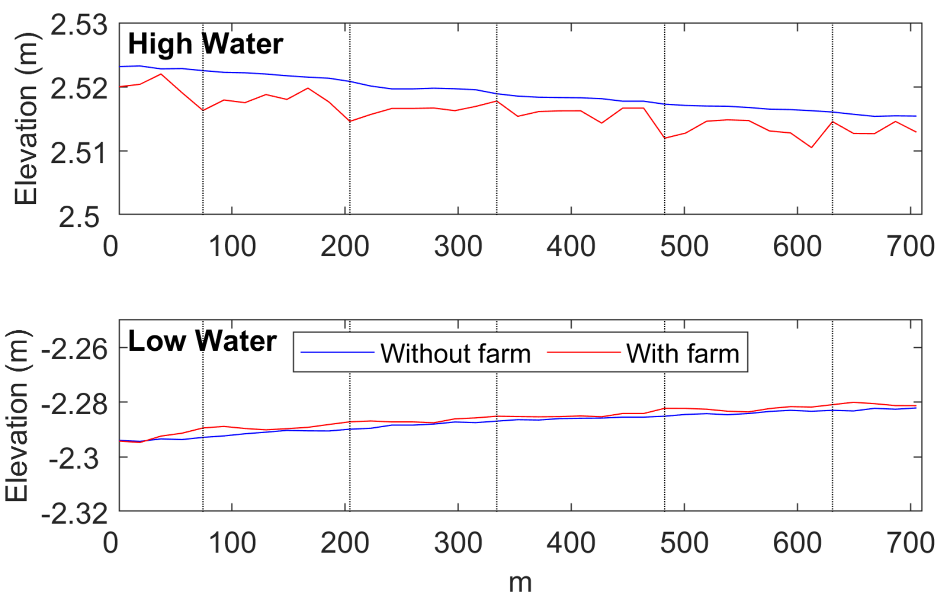

(b) Slice 2

Figure 10: Surface elevation with and without turbine farm along slices 1 and 2 in Figure 5 at HW and LW.

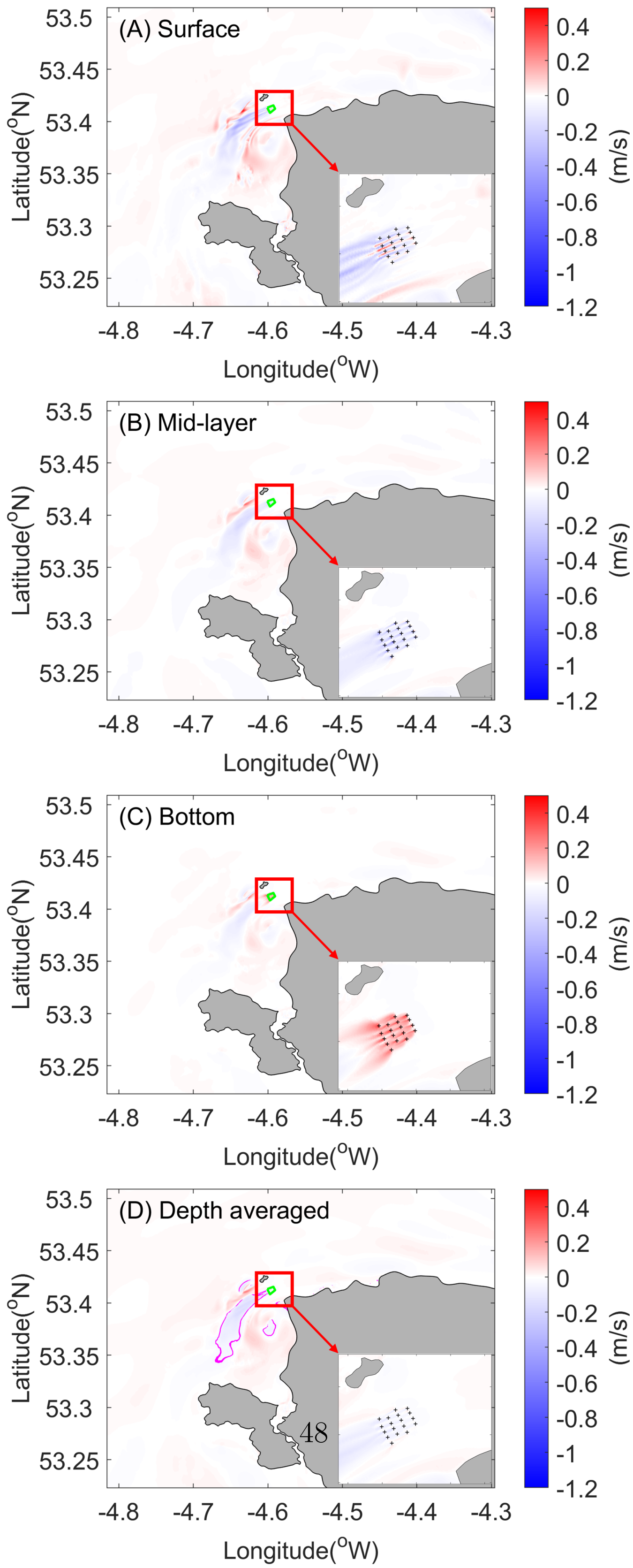

Figure 11: Changes of flow fields at HW.

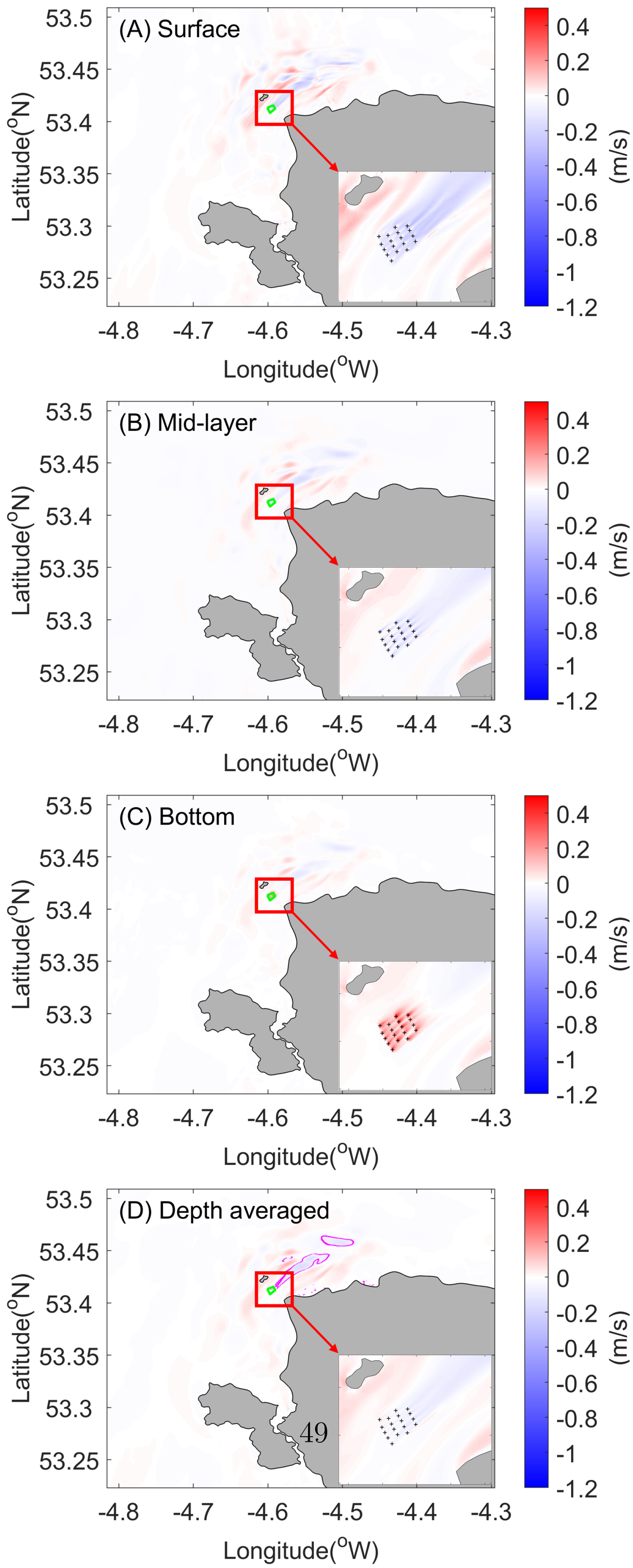

Figure 12: Changes of flow fields at LW.

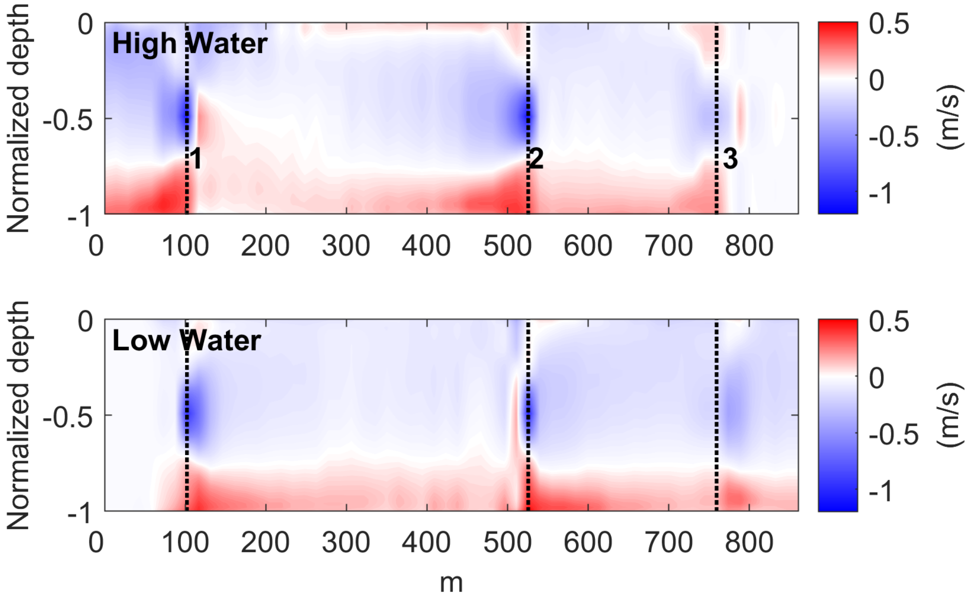

(a) Slice 1

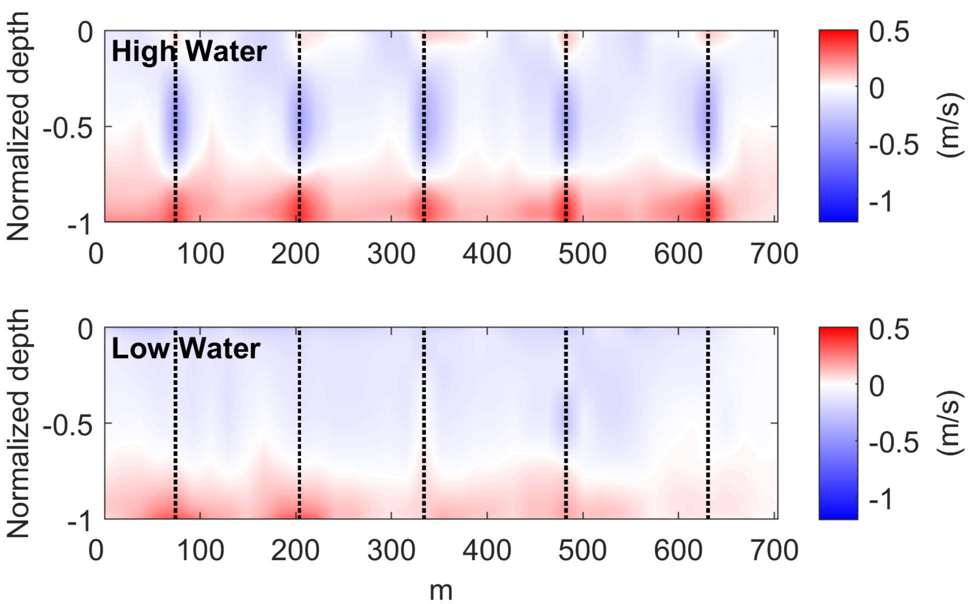

(b) Slice 2

Figure 13: Changes of velocity along slices 1 and 2 in Figure 5 at HW and LW.

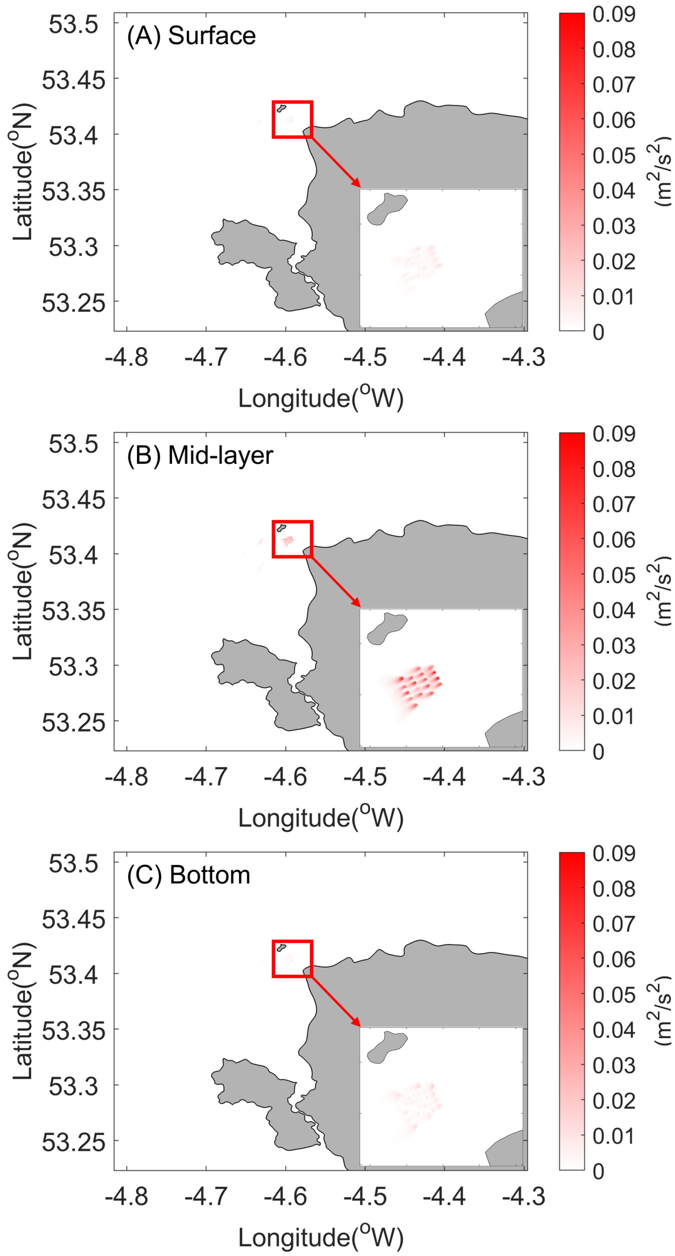

Figure 14: Changes of TKE at HW.

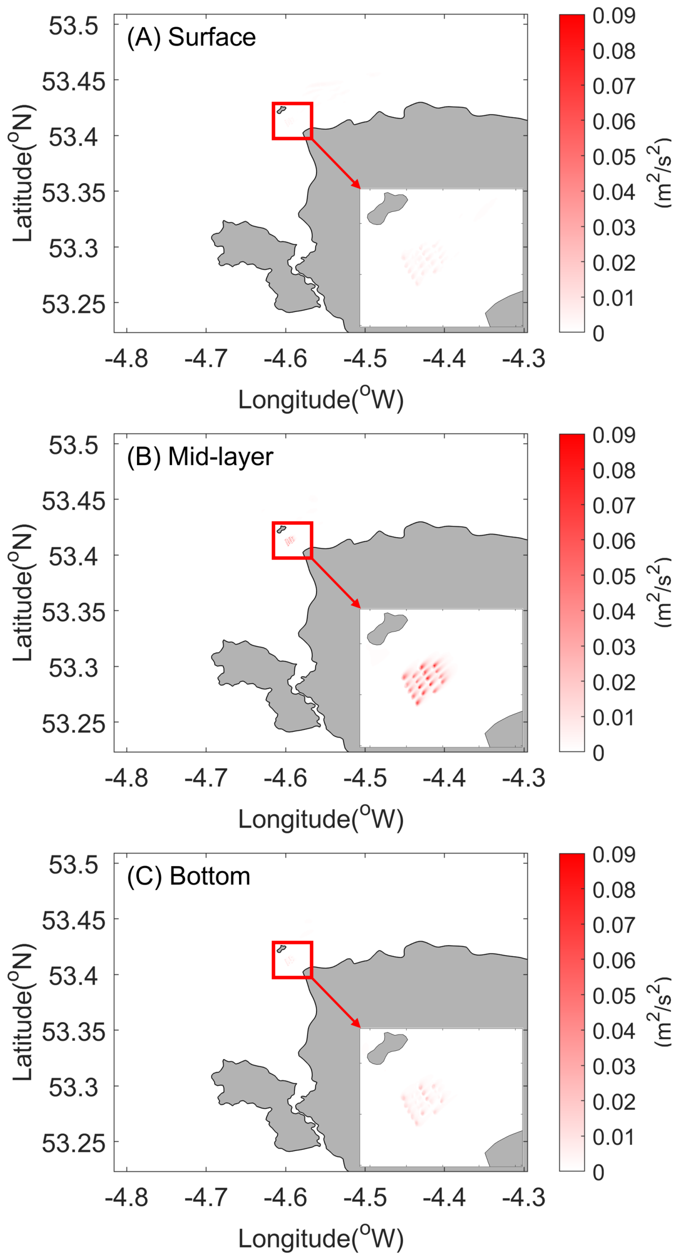

Figure 15: Changes of TKE at LW.

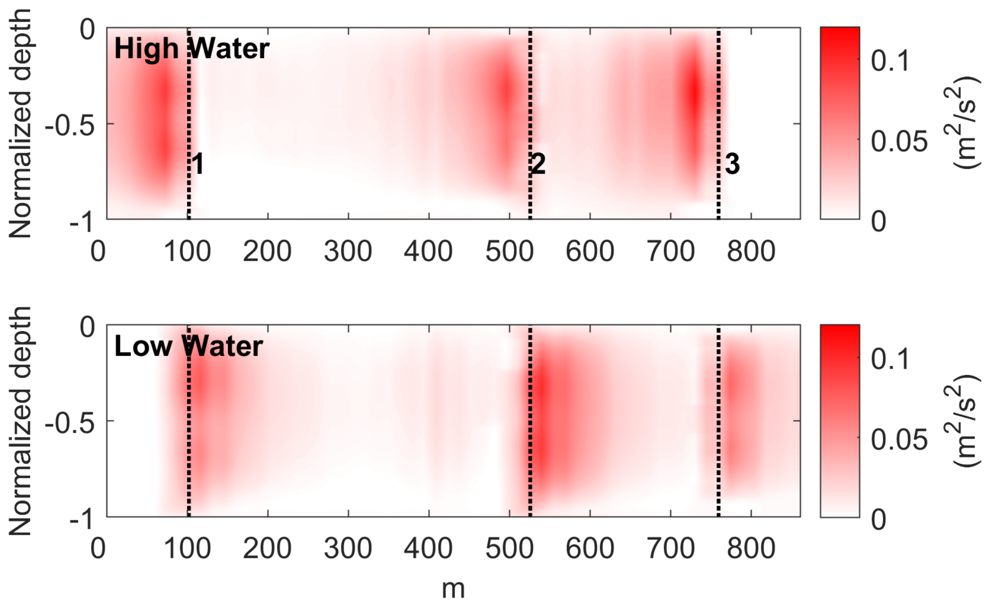

(a) Slice 1

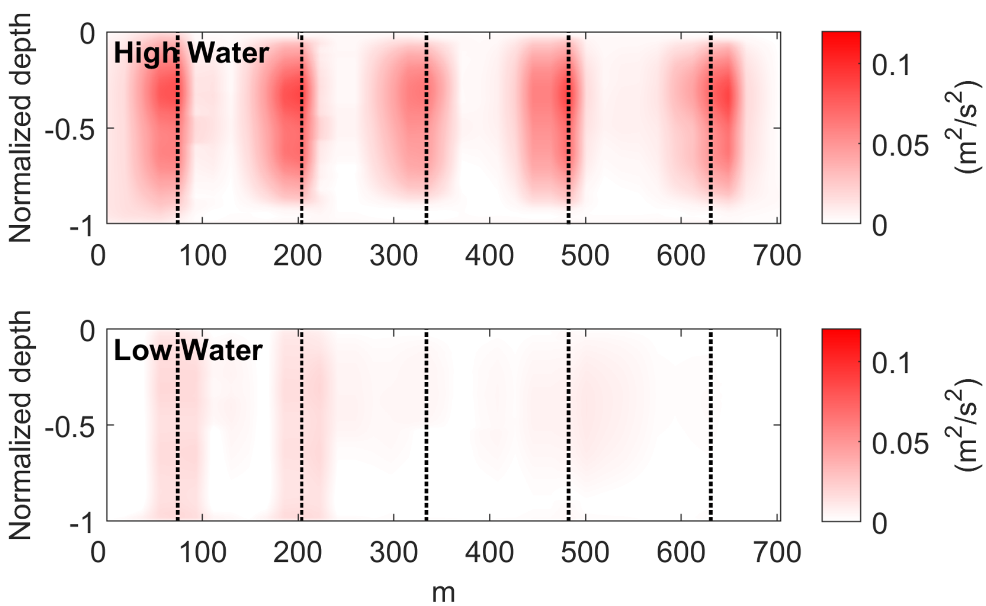

(b) Slice 2

Figure 16: Changes of TKE along slices 1 and 2 in Figure 5 at HW and LW.

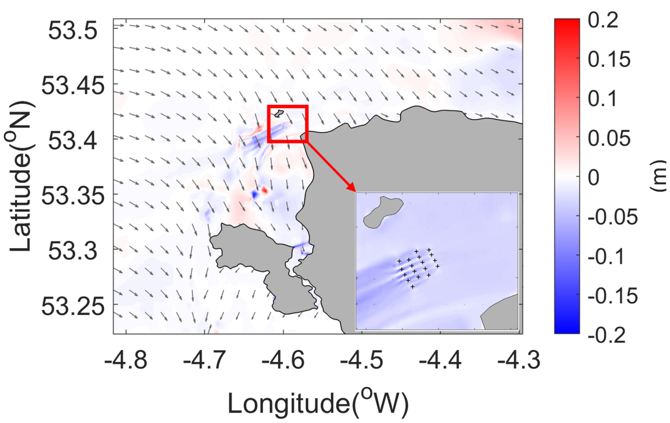

(a) HW

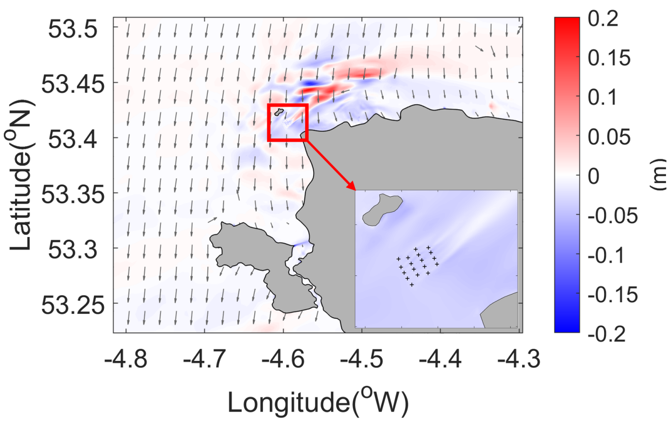

(b) LW

Figure 17: Changes of significant wave height of surface waves. Arrows are imposed to indicate undisturbed wave directions.

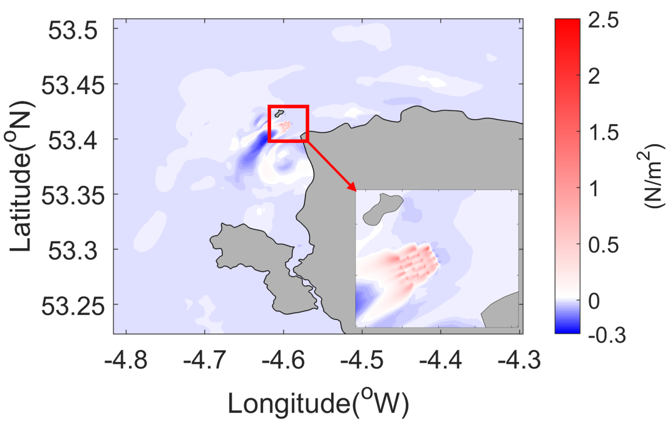

(a) HW

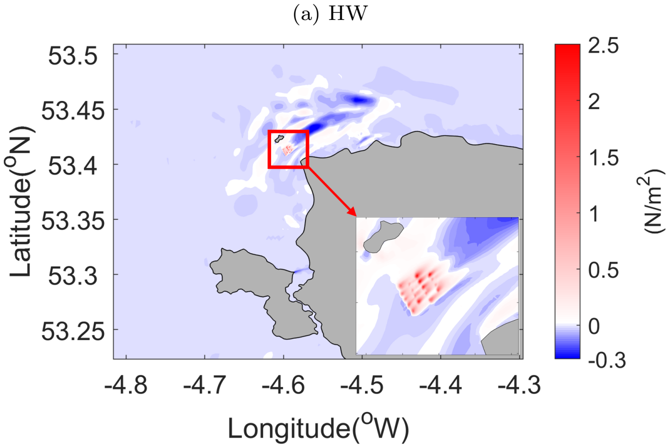

(b) LW

Figure 18: Changes of bed shear stress.

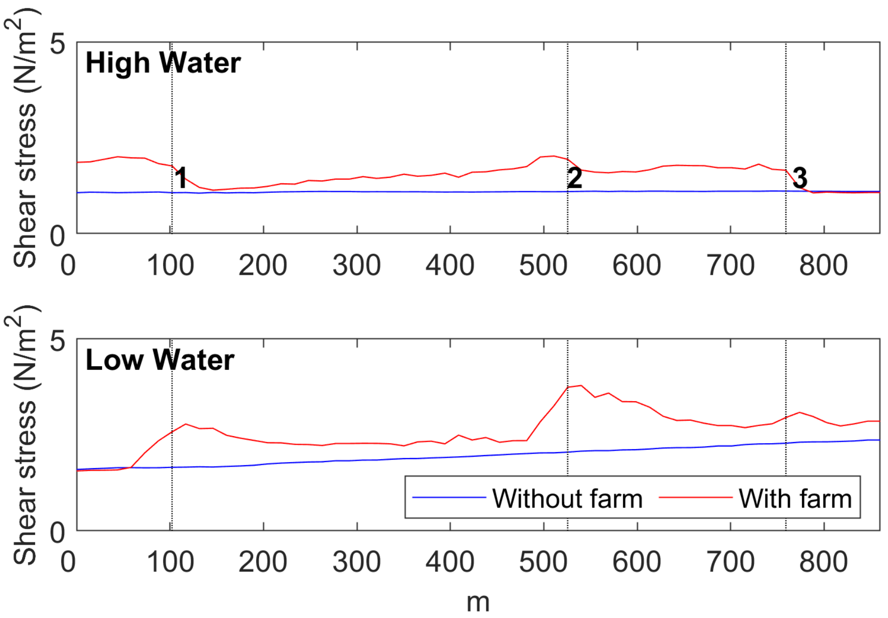

(a) Slice 1

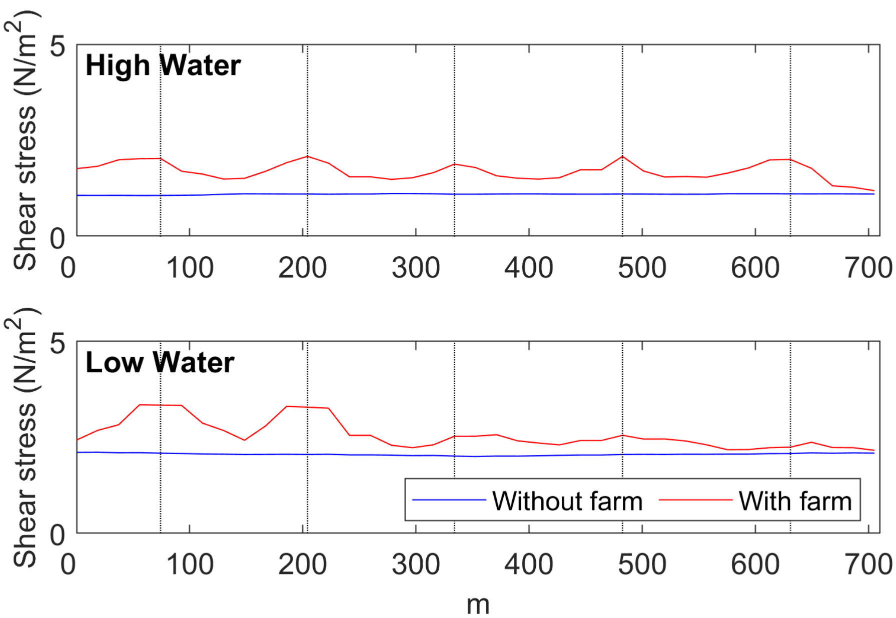

(b) Slice 2

Figure 19: Bed shear stress with and without turbine farm along slices 1 and 2 in Figure 5 at HW and LW.

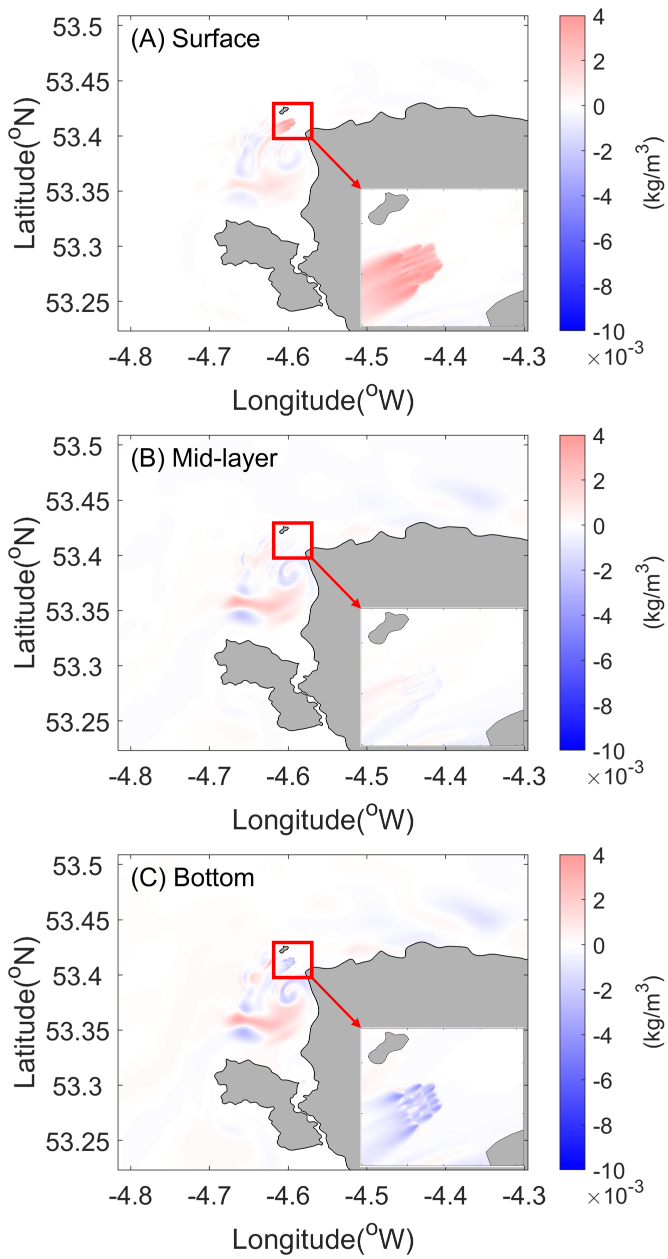

Figure 20: Changes of suspended sediment concentration at HW.

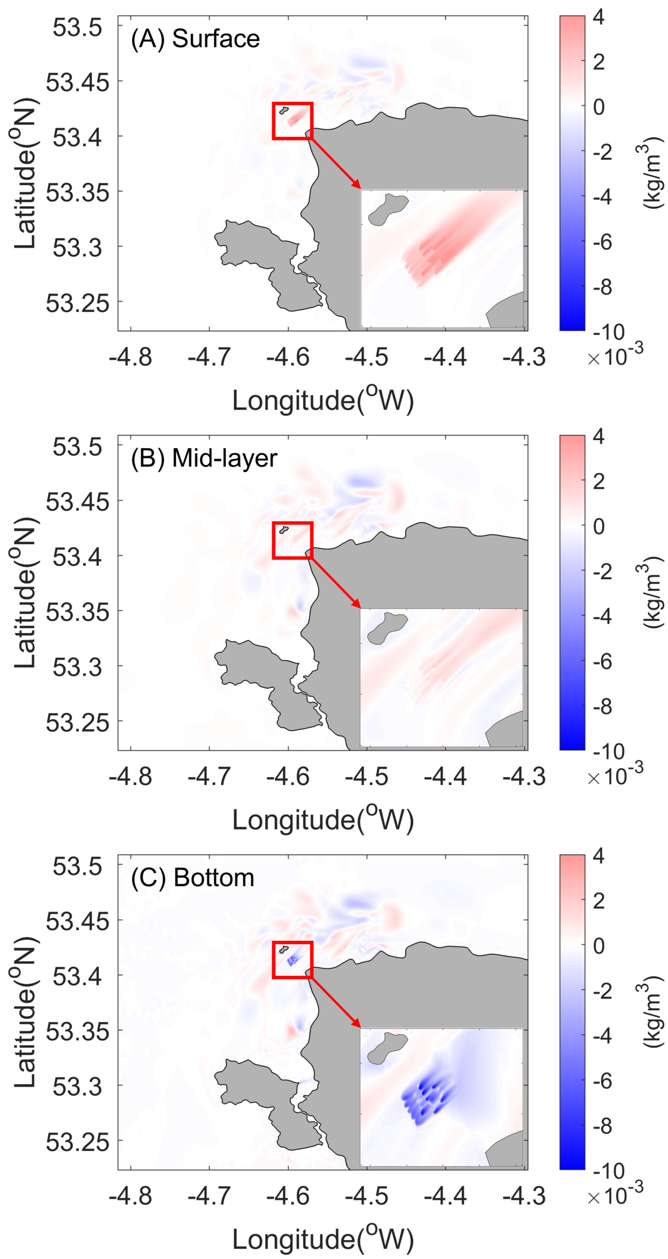

Figure 21: Changes of suspended sediment concentration at LW.

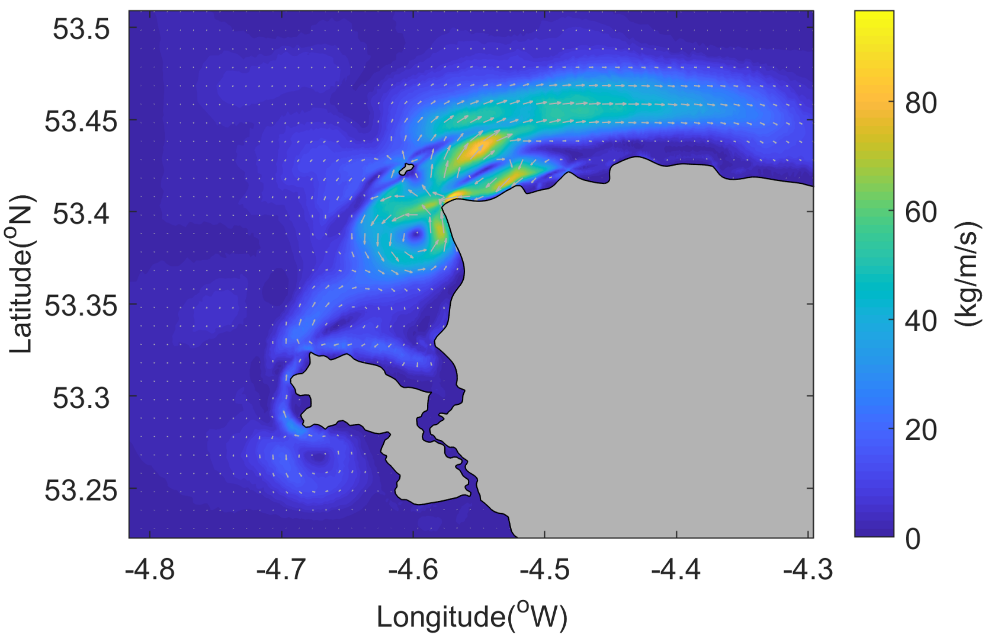

(a) Baseline condition (no turbine)

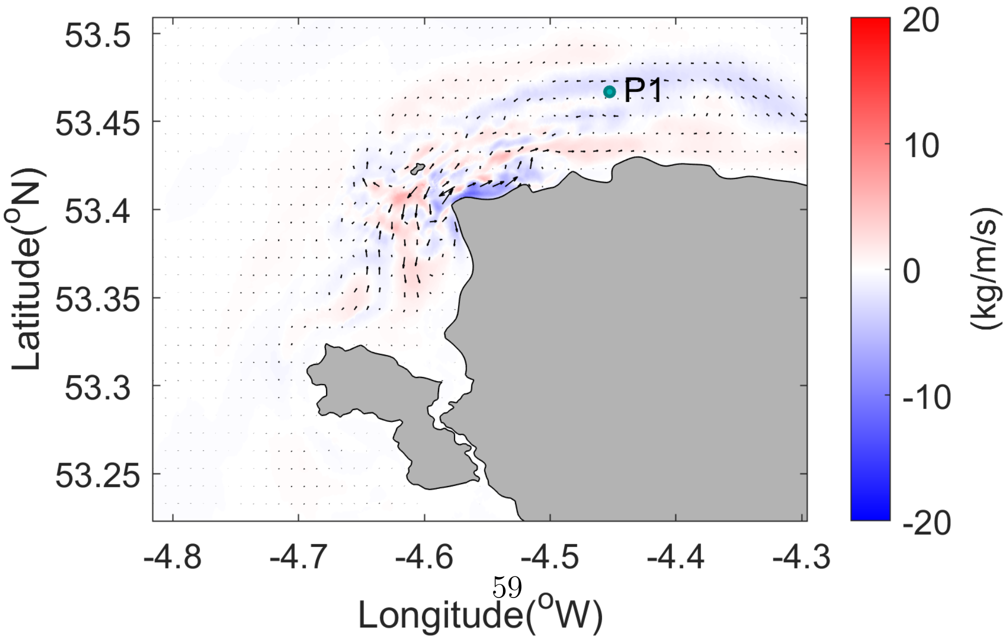

(b) Differences caused by the turbine array

Figure 22: Residual sediment transport pathways around the Anglesey coast.

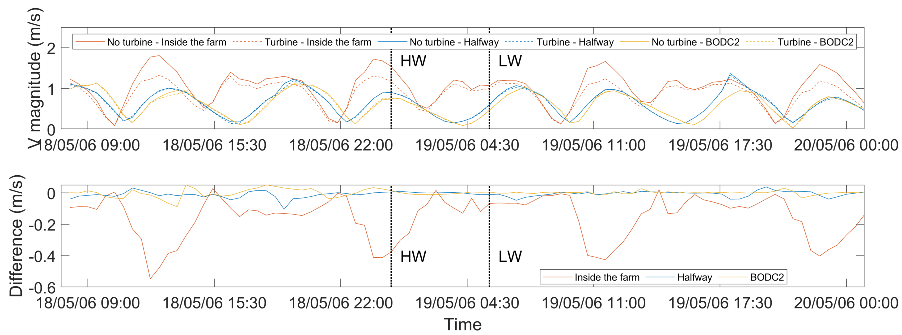

(a) Velocity

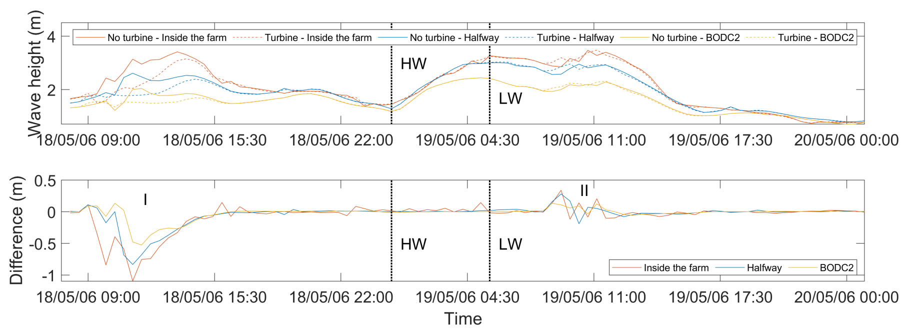

(b) Wave height

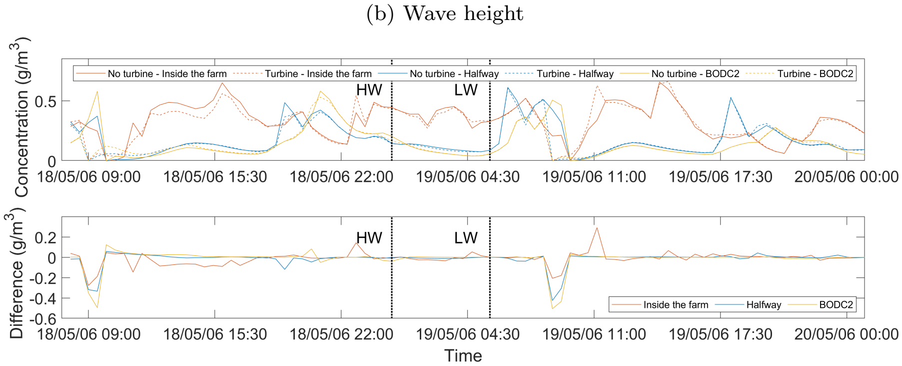

(c) Suspended sediment concentration

Figure 23: Velocity, wave height and suspended sediment concentration with and without the turbine farm and the differences caused by the turbines at the intersect of the two slices in Figure 5, BODC2 in Figure 2 and halfway between these two points, i.e. P1 in Figure 22B, over time.